Cerebellospinal Neurons Regulate Motor Performance and Motor Learning

Anupama Sathyamurthy[1], **Arnab Barik**[2], **Courtney I. Dobrott**[1,4], **Kaya J.E. Matson**[1], **Stefan Stoica**[1], **Randall Pursley**[3], **Alexander T. Chesler**[2], **Ariel J. Levine**[1,5,*]

[1]Spinal Circuits and Plasticity Unit, National Institute of Neurological Disorders and Stroke, National Institutes of Health, Bethesda, MD 20892, USA

[2]Sensory Cells and Circuits Section, National Center for Complimentary and Integrative Health, National Institutes of Health, Bethesda, MD 20892, USA

[3]Signal Processing and Instrumentation Section, Center for Information Technology, National Institutes of Health, Bethesda, MD 20892, USA

[4]Present address: University of Colorado, Aurora, CO 80045, USA

[5]Lead Contact

Graphical Abstract

*Correspondence: ariel.levine@nih.gov.
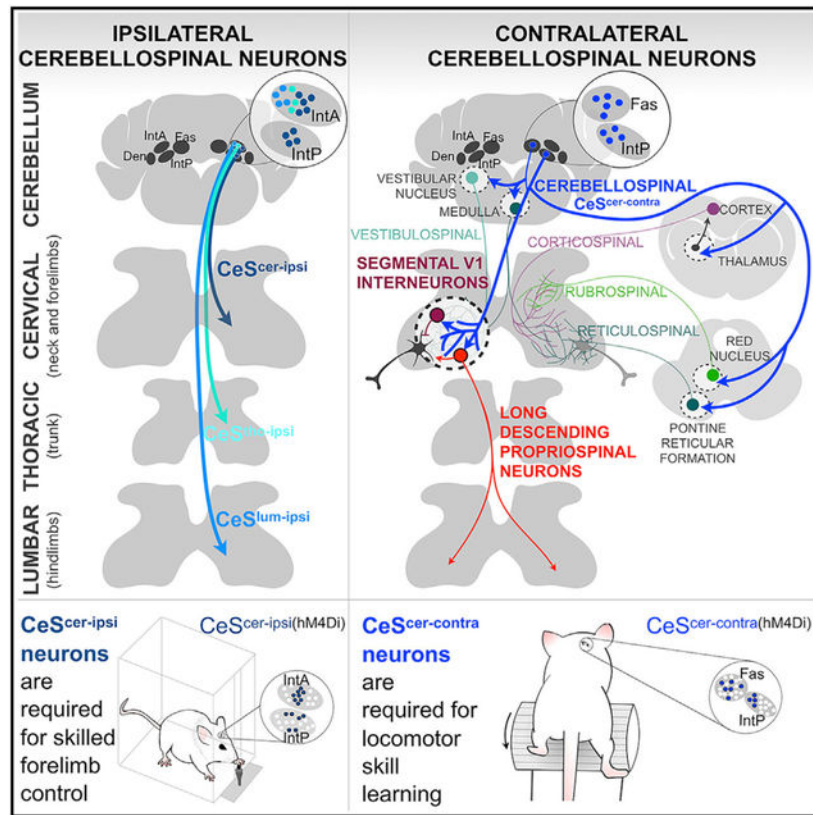
SUMMARY

To understand the neural basis of behavior, it is important to reveal how movements are planned, executed, and refined by networks of neurons distributed throughout the nervous system. Here, we report the neuroanatomical organization and behavioral roles of cerebellospinal (CeS) neurons. Using intersectional genetic techniques, we find that CeS neurons constitute a small minority of excitatory neurons in the fastigial and interpositus deep cerebellar nuclei, target pre-motor circuits in the ventral spinal cord and the brain, and control distinct aspects of movement. CeS neurons that project to the ipsilateral cervical cord are required for skilled forelimb performance, while CeS neurons that project to the contralateral cervical cord are involved in skilled locomotor learning. Together, this work establishes CeS neurons as a critical component of the neural circuitry for skilled movements and provides insights into the organizational logic of motor networks.

In Brief

Sathyamurthy et al. define the organization, function, and targets of cerebellospinal neurons, revealing a direct link between the deep cerebellar nuclei and motor execution circuits in the spinal cord and demonstrating a role for these neurons in motor control.

INTRODUCTION

Seamless movements are accomplished by the concerted action of diverse motor areas, including the cortex, basal ganglia, red nucleus, brainstem, cerebellum, and spinal cord. Over the past century, there have been great strides toward defining the neural computations of each of these areas and their contribution to motor control. However, to truly understand the neural basis of behavior, it is essential to reveal how individual motor areas are bound into coordinated networks to accomplish purposeful movement. All neural information must flow through the "final common pathway" of spinal motoneurons to drive movement (Sherrington, 1911). While motor areas in the brain may encode discrete aspects of movement such as the neural commands for the initiation, speed, and direction of movement, the spinal cord integrates and transforms these complementary motor commands into precise patterns of muscle contractions (Armstrong, 1986; Shik and Orlovsky, 1976). The intricate processing capabilities of the cord are sustained by a diverse array of functionally specialized interneurons, which serve as rich substrates for finetuning, diversifying, and coordinating motor output (Jankowska, 1992). Therefore, deconstructing motor circuits with reference to their terminal targets among spinal networks can provide a powerful framework for decoding the neural mechanisms underlying motor control.

To exert precise temporal and spatial control over the body's musculature, it is essential to accurately time the neural activity of multiple motor areas, a task that is thought to be served by the cerebellum (Arshavsky et al., 1983). Indeed, loss of motor coordination or ataxia is a hallmark of cerebellar damage (Holmes, 1917; Sprague and Chambers, 1953; Carrea and Mettler, 1947). This critical role for the cerebellum in motor coordination is attributed to its ability to learn and predict errors and to ultimately transform error predictions into corrected motor commands (Wolpert et al., 1998). However, the organizational logic of efferent cerebellar pathways that convey cerebellar computations to the appropriate spinal segments for movement are not clear (Thach et al., 1992). Nearly all cerebellar output flows from Purkinje neurons to the rest of the nervous system via the deep cerebellar nuclei (DCN): the dentate, fastigial, and interpositus nuclei (Thach et al., 1992). Rather than acting as passive relays, these nuclei integrate sensori-motor information and play essential roles in motor control (Becker and Person, 2019; Brooks et al., 2015; Chabrol et al., 2019; Low et al., 2018; Martin et al., 2000; Mason et al., 1998; Mori et al., 1999; Perciavalle et al., 2013; Sprague and Chambers, 1953; Strick et al., 2009; Yu and Eidelberg, 1983). DCN neurons project to the thalamus, red nucleus, and brainstem nuclei, sites where cerebellar instructions are likely integrated with other sensori-motor information and relayed to spinal circuits that execute movements. (Angaut and Bowsher, 1965; Asanuma et al., 1983; Batton et al., 1977; Brodal and Szikla, 1972; Courville, 1966; Kelly and Strick, 2003; Tolbert et al., 1980). Accordingly, most contemporary and classic studies of motor control have posited that the cerebellum influences movement *only* through indirect, poly-synaptic relays in these brain areas (Kandel, 2013; Perciavalle et al., 2013; Ruigrok, 2012). However, a direct projection from the DCN to the spinal cord has been reported.

Beginning with anatomical circuit tracing studies over a century ago, direct cerebellospinal (CeS) neurons have been observed in a wide variety of tetrapod animals (Asanuma et al., 1980; Cajal, 2012; Carrea and Mettler, 1954; Fukushima et al., 1977; Gray, 1926; Jakob,

1942; Liang et al., 2011; Matsushita and Hosoya, 1978; Nudo and Masterton, 1988; Thomas et al., 1956; Wang et al., 2018; Wilson et al., 1978), but their initial descriptions were debated (Barker, 1901; Gray, 1918). Nevertheless, anatomical descriptions of the CeS pathway were corroborated by electrophysiological recordings (Alstermark et al., 1987; Orioli, 1961; Wilson et al., 1978). Notably, despite the potential importance of CeS neurons in mediating movement, these neurons remain poorly characterized and have not been incorporated into the framework for studies of motor control.

Here, we investigated the anatomy, function, and targets of CeS neurons in the adult mouse and reveal that they play critical roles in motor performance and motor learning. We first defined three groups of excitatory CeS neurons based on their location within the DCN and their pattern of connectivity with the spinal cord. Next, we found that CeS neurons that project to the ipsilateral cervical spinal cord are critical for skilled forelimb movement, while those that project to the contralateral cervical spinal cord are important for skilled locomotor learning. Finally, we found that CeS neurons target segmental and long-range intersegmental neurons in the cervical cord, thereby providing a direct link between the cerebellum and spinal substrates for motor coordination. Together, this work establishes CeS neurons as important players in the descending control of movement.

RESULTS

A Neuroanatomical Characterization of CeS Neurons

We first sought to elucidate the basic neuroanatomical features of CeS neurons. To reliably identify and label CeS neurons, we used a recently developed retrograde viral labeling tool, rAAV2-retro, that offers an efficient way to retrogradely label neurons when delivered to their target locations (Tervo et al., 2016). We injected rAAV2-retro:EBFP-Cre bilaterally into the cervical region of Cre-dependent fluorescent reporter mice (Figure 1A) and found retro-labeled neurons within the cortex, red nucleus, vestibular nucleus, and discrete nuclei in the medullary and pontine reticular formation. These are well-known sources of direct descending inputs to the spinal cord, thereby attesting to the reliability of this viral tool for labeling descending neurons (Figures 1B and S1A–S1G). Within the cerebellum, we found pre-spinal cells in the interpositus and fastigial DCN (Figure 1C) (n = 9 mice), thereby corroborating the existence of a direct CeS tract to the cervical spinal cord, which controls the neck and forelimbs. Since distinct regions of the spinal cord control different parts of the body, we sought to determine if the thoracic and lumbar segments—which control the trunk and the hindlimbs, respectively—are also targeted by CeS neurons. To address this, we retrogradely labeled neurons projecting to the thoracic (n = 4 mice) and lumbar regions (n = 7 mice), and in each case, we found retro-labeled neurons enriched in the interpositus nucleus, indicating that the DCN communicate with all major motor divisions of the cord (Figures S1L–S1P).

Since DCN differ from each other in terms of connectivity and function (Clarke and Horsley, 1905; Jansen and Brodal, 1940; Thach et al., 1992), we comprehensively mapped the distribution of pre-cervical and pre-lumbar CeS neurons within these nuclei. Unilateral injection of rAAV2-retro virus expressing either nuclear-localized GFP or mCherry fluorescent protein into the cervical (n = 7 mice) and lumbar regions (n = 4 mice) revealed

clear distinctions in the organization of CeS neurons projecting to the ipsilateral and contralateral halves of the cervical and lumbar spinal cord (Figures 2A, 2B, and S2A–S2C). Neurons retro-labeled from the cervical region were enriched in the ipsilateral anterior interpositus nucleus (IntA) (42% of all pre-cervical CeS neurons) and the contralateral fastigial (18%) and posterior interpositus nuclei (IntP) (18%), while those labeled from the lumbar region were enriched in the ipsilateral IntA (90% of all pre-lumbar CeS neurons), suggestive of anatomical specificity and functional diversity of CeS neurons. Moreover, precervical and pre-lumbar CeS neurons were clearly segregated within the IntA. While pre-cervical CeS neurons were located in the middle third of the IntA, pre-lumbar CeS neurons were confined to the medial third of this nucleus (Figure 2B, row 2). This somatotopic segregation of CeS neurons is a general pattern shared with pre-spinal neurons in the motor cortex and red nucleus (Figures S1H–S1K).

Next, we estimated the prevalence of CeS neurons among the DCN in which they reside and found that pre-cervical and prelumbar CeS neurons constitute a small proportion (~5%–10%) of neurons in their respective DCN (Figures 2C and S2D), indicating that only a small minority of DCN neurons have direct access to spinal circuits.

Finally, how do CeS neurons compare to previously described DCN cell types, which have been categorized by neurotransmitter status and size (Bagnall et al., 2009; Uusisaari and Knöpfel, 2012)? Analysis of the neurotransmitter status of these neurons using fluorescence *in situ* hybridization (FISH) revealed that 97% of CeS neurons (367 neurons from two mice) co-expressed the glutamatergic marker, *Slc17a6*, indicative of the excitatory phenotype of these neurons (Figures 1D–1F). In addition, we found that the mean area occupied by CeS neurons was 254 ± 2 μm^2 and that the mean diameter was 24 ± 1 μm (Figures S2E–S2H; n = 1942 neurons from seven mice), which roughly corresponds to a subset of the "large" category of presumptive excitatory neurons in the DCN (Canto et al., 2016; Chan-Palay, 2013; Uusisaari et al., 2007), in keeping with our FISH results.

Overall, these results indicate that CeS neurons represent a small, somatotopically organized population of excitatory DCN neurons and contact each of the major regions of the spinal cord. Based on laterality and connectivity patterns with the spinal cord, we classified them into three groups: (1) an ipsilateral group that targets the cervical spinal cord (CeS^cer-ipsi), (2) a contralateral group that targets the cervical spinal cord (CeS^cer-contra), and (3) a smaller ipsilateral group that targets the lumbar spinal cord (CeS^lum-ipsi) (Figure 2D). These studies establish an anatomical framework for functional studies of CeS neurons.

CeS^cer-ipsi Neurons Are Required for Skilled Forelimb Movement

Next, we sought to elucidate the function of CeS neurons. The topographic organization of direct inputs from the DCN to the spinal cord provides powerful experimental access points to dissect the function of specific subsets of CeS neurons. Accordingly, we leveraged CeS topography to specifically manipulate the two distinct populations of pre-cervical neurons, CeS^cer-ipsi and CeS^cer-contra. Unilateral injections of rAAV2-retro:Cre virus into the cervical spinal cord combined with injections of Cre-dependent hM4Di (Roth, 2016; Zhu et al., 2014) into either the ipsilateral or contralateral DCN allowed specific silencing of these CeS neurons (Figures 3A–3C, 4A, and 4B).

While the interpositus nuclei are known to be necessary for skilled forelimb control (Becker and Person, 2019; Chambers and Sprague, 1955; Cooper et al., 2000; Low et al., 2018; Martin et al., 2000; Milak et al., 1997; Uno et al., 1973), the underlying neural substrates have remained obscure. We hypothesized that the small, specific fraction of interpositus neurons that project directly to the ipsilateral cervical spinal cord ($CeS^{cer-ipsi}$ neurons) would represent a critical component of the circuitry. To test the requirement for $CeS^{cer-ipsi}$ neurons in mediating interpositus' role in skilled forelimb movement, we silenced their activity using virally delivered pharmacogenetics and subjected the mice to a classic single-pellet retrieval assay (Figures 3A–3D; Castro, 1972; Whishaw et al., 2008).

We found that silencing $CeS^{cer-ipsi}$ neurons significantly impaired the ability of mice to perform skilled pellet retrieval. Control (vehicle-treated) mice displayed progressive improvement in successful pellet retrievals over several days of training, while CNO (clozapine N-oxide) treated mice did not improve their performance (Figure 3E). To determine if the inability to successfully perform the task was confined to a specific phase of the movement, we visually scored the three major phases of pellet retrieval: the outward reach movement guiding the arm toward the pellet, the grasping of the pellet, and the retraction of the arm to bring the pellet to the mouth for eating (Video S1). In both groups of mice, very few trials (<3%) involved a complete inability to guide the arm to the vicinity of the pellet. While control mice were able to successfully grasp the pellet and retract the arm to put the pellet in the mouth, CNO-treated mice often missed the pellet and, instead, inadvertently dislodged it. However, in trials in which these mice did secure the pellet, they did not display an increase in the frequency of drops compared to controls (Figure S3B). CNO treatment alone on wild-type mice had no effect on skilled reaching performance (Figure S3C).

The deficiency in skilled reaching could reflect a failure to properly learn new movements over time, or it could reflect an acute failure of motor control and coordination, and the cerebellum has been implicated in both of these functions. To distinguish between these two possibilities, we trained mice to perform skilled reaching and delivered CNO only on day 10, when the mice were already proficient at the task. Similar to results described above, post-learning delivery of CNO caused a significant decrease in the number of successful trials (Figure 3F), suggesting that $CeS^{cer-ipsi}$ neurons are necessary for online control of the forelimb during skilled movement. Analyses of the different phases showed that in most control trials (vehicle treatment), mice were able to perform each movement phase and to seamlessly progress through each of these phases to successfully retrieve the pellet. In contrast, in CNO-treated trials, mice took longer to successfully guide the arm to the vicinity of the pellet (the duration from liftoff to complete extension of digits/touching the pellet) (Figure 3J; Videos S2 and S3). This is similar to the motor deficits observed in patients with acute cerebellar damage (Konczak et al., 2010; Zackowski et al., 2002) and in experimental animals models upon silencing or cooling of the interpositus nuclei (Cooper et al., 2000; Martin et al., 2000; Milak et al., 1997; Uno et al., 1973). Despite the increased reach duration, these mice were able to successfully guide the arm to the vicinity of the pellet (Figure 3G). However, they subsequently failed to retrieve the pellet (Figure 3H; Videos S2 and S3). This failure did not stem from an inherent inability to perform the grasp motion, because mice often progressed through the grasp phase despite missing the pellet. Instead,

failure to retrieve the pellet appeared to be due to an inability to temporally or spatially coordinate the grasp motion to achieve endpoint precision (Figures 3H and 3I). Overall, these results suggest that CeS$^{cer\text{-}ipsi}$ neurons are necessary for seamlessly executing skilled forelimb movements.

Finally, to test whether this effect was specific to reaching or if it reflected a broader motor deficit, we treated mice that expressed hM4Di in CeS$^{cer\text{-}ipsi}$ neurons with CNO or vehicle and observed their motor behaviors in the home cage and tested them on a battery of motor tasks but did not find any differences between the two groups (Figures S3D–S3I). These data demonstrate that a small group of neurons in the interpositus nuclei, CeS$^{cer\text{-}ipsi}$ neurons, are specifically necessary for skilled pellet retrieval and suggest that the interpositus nuclei rely on CeS neurons to exert their role in forelimb control.

CeS$^{cer\text{-}contra}$ Neurons Are Required for Locomotor Learning

Next, we sought to discern the function of contralaterally projecting CeS neurons (CeS$^{cer\text{-}contra}$) (Figures 4A and 4B). These neurons are localized to the fastigial and IntP nuclei, which act in concert with their input zones—the vermis and the paravermis, respectively—to exert proximal limb and trunk control (Carrea and Mettler, 1947; Chambers and Sprague, 1955; Darmohray et al., 2019; Yu and Eidelberg, 1983). Given this, we hypothesized that silencing these neurons would produce ataxia and adversely affect balance, posture, and locomotion. Surprisingly, we found that silencing these neurons did not affect locomotor gait parameters (Figures S4B–S4D) and did not alter the time to cross wide or narrow beams (a skill that requires balance) (Figures 4D and 4E). Moreover, in contrast to silencing CeS$^{cer\text{-}ipsi}$ neurons, we found that silencing CeS$^{cer\text{-}contra}$ neurons had no effect on skilled limb control in a single-pellet retrieval task (Figure 4C).

We next considered that these neurons may be necessary for more challenging skilled locomotor tasks. To test this, we subjected the mice to an accelerating rotarod task, a skilled locomotor task in which mice are tested on their ability to adjust their gait and posture to stay on an accelerating rod (Buitrago et al., 2004; Dunham and Miya, 1957) (Figure 4F). While vehicle-treated animals improved and spent increasing amounts of time on the rod over successive trials and days of testing, animals that received CNO were impaired in their ability to sustain skilled locomotion on the rotarod (Figure 4G). We observed similar results upon using alternative strategies to silence (rAAV2:KORD, a pharmacogenetic neuronal silencer that is controlled by the drug salvinorin) (Vardy et al., 2015) or ablate (rAAV2:DTA, a toxin) (Wu et al., 2014) CeS$^{cer\text{-}contra}$ neurons (Figures S4F–S4I). CNO treatment or salvinorin treatment alone had no effect on rotarod performance (Figure S4E; Vardy et al., 2015).

This impairment in motor performance could reflect an acute requirement for activity in CeS$^{cer\text{-}contra}$ neurons during motor skill execution, or it could reflect a role for these neurons in the acquisition of the skill. To dissociate between these two possibilities, we allowed mice that expressed hM4Di in the CeS$^{cer\text{-}contra}$ neurons to train normally on rotarod with daily vehicle injections and then treated these mice with CNO after learning had occurred. Strikingly, we found that manipulating these neurons once the task had already been learned

did not affect rotarod performance (Figure 4H). Together, these data uncovered the requirement for CeS$^{cer\text{-}contra}$ neurons in the learning phase of a skilled locomotor task.

The CeS$^{cer\text{-}contra}$ Tract Targets Spinal Neurons That Mediate Limb Coordination

To gain insights into the circuit mechanisms underlying the role of CeS$^{cer\text{-}contra}$ neurons in skilled locomotor learning, we sought to identify the spinal termination zone and post-synaptic partners of the CeS$^{cer\text{-}contra}$ tract. To map the axon trajectory and synaptic terminals of CeS$^{cer\text{-}contra}$ neurons, we used an intersectional viral labeling strategy, which allowed selective labeling of these neurons with the fluorescent reporter protein, mCherry, or synaptophysin fused to eGFP, respectively. We found that the axons of CeS$^{cer\text{-}contra}$ neurons exited the IntP and fastigial nuclei, crossed the midline within the cerebellar commissure (above the fourth ventricle), and descended in the medial brainstem before entering the cord and traveling within the ventral funiculus (Figures S5A–S5C).

Since laminar identity and dorso-ventral position of spinal neurons correlate well with function (reviewed in Levine et al., 2012), we focused on the termination pattern of CeS$^{cer\text{-}contra}$ neurons in the spinal gray matter. We observed axons and synaptic terminals of CeS$^{cer\text{-}contra}$ neurons in the medial portion of the ventral horn (lamina VII and VIII), which contains both local segmental and long-range intersegmental pre-motor neurons (Figures 5A– 5C and S5C–S5F; Jankowska, 1992; Watson et al., 2009). Within this termination zone, synaptic terminals of CeS$^{cer\text{-}contra}$ neurons were closely apposed to the post-synaptic density of spinal neurons (Figure 5C). Roughly 73% of neurons targeted by CeS$^{cer\text{-}contra}$ terminals were in lamina VIII, followed by 24% of neurons in lamina VII. Lamina IX, where motoneurons reside, was largely devoid of CeS$^{cer\text{-}contra}$ terminals (Figure 5D). No synaptic terminals were seen on the proximal dendrites or soma of large ChAT+ alpha motoneurons, suggesting that CeS$^{cer\text{-}contra}$ neurons are unlikely to synapse onto these cells. The negligible fraction of lamina IX neurons receiving CeS$^{cer\text{-}contra}$ input were presumptive gamma motoneurons, identified based on their location in lamina IX, small size, ChAT expression, and lack of NeuN (Figures S5G and S5H; Friese et al., 2009). While these inputs could account for the observation that some cervical motoneurons receive short-latency excitatory input from the contralateral fastigial nucleus in the cerebellum (Wilson et al., 1978), it is unlikely that they mediate the behavioral role of CeS$^{cer\text{-}contra}$ neurons.

Next, we reasoned that the lack of improvement in skilled locomotor performance might reflect an inability to coordinate the activity of the major body regions: neck, forelimbs, trunk, and hindlimbs. This prompted us to consider two distinct subpopulations of spinal neurons: (1) segmental pre-motor neurons that innervate neck and forelimb motoneurons at cervical levels; and (2) long descending propriospinal neurons, whose soma reside at cervical levels but whose axons innervate pre-motor and motor neurons in the thoracic and lumbar segments of the spinal cord, which control the trunk and the limbs, respectively (Flynn et al., 2017; Miller and van der Burg, 1973; Ni et al., 2014; Ruder et al., 2016; Sherrington and Laslett, 1903; Skinner et al., 1979).

First, we tested whether CeS$^{cer\text{-}contra}$ neurons target the V1 class (Engrailed (En1) lineage) of segmental, local inhibitory neurons (Briscoe et al., 2000; Saueressig et al., 1999), sub-types of which provide mono-synaptic input to ipsilateral motoneurons (Bikoff et al., 2016;

Wenner and O'Donovan, 1999) for three reasons. First, contralateral fastigial stimulation can evoke inhibitory synaptic potentials in cervical motoneurons, even after descending pathways in the medial longitudinal fasciculus of the brain have been lesioned (Matsuyama and Jankowska, 2004; Wilson et al., 1978), suggesting that local inhibitory spinal neurons relay this input. Second, previous studies have shown that ablating V1 cells perturbs locomotor performance at higher speeds on an accelerating rotarod (Gosgnach et al., 2006), similar to the phenotype we observed upon cumulative silencing of CeS$^{cer\text{-}contra}$ neurons. And third, the ventral limit of V1 distribution covaried with the target domain of CeS$^{cer\text{-}contra}$ synaptic terminals, especially at rostral levels. To test if En1-derived V1 neurons receive synaptic input from CeS$^{cer\text{-}contra}$ neurons, we analyzed CeS$^{cer\text{-}contra}$ terminals in En1:Cre;Ai14 tdTomato mice, in which En1-lineage neurons express the fluorescent tdTomato reporter protein (Figures 5E–5G). Indeed, we observed many direct CeS$^{cer\text{-}contra}$ synaptic contacts onto V1 neurons, with ~30% of all V1 neurons in lamina VIII receiving CeS$^{cer\text{-}contra}$ input (Figure 5G). In contrast, excitatory Chx10-expressing V2a neurons, which have also been implicated in regulating the speed of locomotor rhythm (Ampatzis et al., 2014; Crone et al., 2009; Kimura et al., 2006), were only infrequently targeted by CeS$^{cer\text{-}contra}$ neurons (Figure S5I).

Next, we tested if CeS$^{cer\text{-}contra}$ neurons synapse onto long descending propriospinal (LDP) neurons. We labeled LDP neurons by injecting rAAV2-retro:Cre into the lumbar spinal cord of Cre-dependent Ai14 tdTomato reporter mice and labeled CeS$^{cer\text{-}contra}$ terminals in the same mice by injecting rAAV:FLP into the cervical spinal cord and a FLP-dependent rAAV:Synaptophysin/GFP into the contralateral DCN (Figures 5H–5J). We then examined GFP$^+$ synaptic terminals onto tdTomato$^+$ cell bodies in the cervical spinal cord (Figure 5I) and found that 44% (44% ± 5%, mean ± SEM, n = 4 mice) of cervical LDP neurons received inputs from CeS$^{cer\text{-}contra}$ neurons (Figure 5J).

In summary, CeS$^{cer\text{-}contra}$ neurons, which originate in the IntP and fastigial nuclei, target specific classes of local and long-range spinal neurons—including cervical V1 interneurons —which contribute to neck and forelimb control and descending propriospinal neurons, which coordinate forelimb-hindlimb movements. These results delineate two complementary spinal targets of CeS$^{cer\text{-}contra}$ neurons, which could be recruited as ensembles to coordinately regulate multiple body segments and may thereby mediate the role of CeS$^{cer\text{-}contra}$ neurons in skilled locomotion.

An Integrated Network for Cerebellar Output to Spinal Motor Circuits

It is well established that descending pathways to the spinal cord collateralize extensively within the brain and likely act through distributed networks of downstream neural populations. Accordingly, we examined if CeS$^{cer\text{-}contra}$ neurons target motor areas in the brain (Figures 6, S6C, S6D, S6F, S6H, and S6J) and found axons and pre-synaptic terminals of CeS$^{cer\text{-}contra}$ neurons in regions of the midbrain and brainstem that give rise to the rubrospinal, reticulospinal, and vestibulospinal descending pathways, including the red nucleus, the pontine reticular nucleus, the medullary reticular formation, and the lateral vestibular nucleus (Figures 6B–6D). Notably, CeS$^{cer\text{-}contra}$ terminals were absent in the inferior olive, which is known to receive input only from inhibitory DCN neurons (De

Zeeuw et al., 1998; Figures S6I and S6J). We also observed CeS$^{cer\text{-}contra}$ collaterals in the cerebellar cortex (Figure 6A) and the ventral postero-medial/ lateral thalamus (Figure S6F), which is known to relay cerebellar output to the motor cortex. Lastly, we observed dense CeS$^{cer\text{-}contra}$ collaterals in the reticulotegmental nucleus (TRN) in the pons (Figure 6C), tracing a recurrent loop from the DCN to the cerebellar cortex via this nucleus (Brodal and Szikla, 1972). To estimate the degree of collateralization of CeS$^{cer\text{-}contra}$ neurons in the brain, we performed dual labeling experiments and found that approximately 50%, 27%, and 47% of CeS$^{cer\text{-}contra}$ neurons also projected to the contralateral thalamus, the midbrain/red nucleus, or the medulla (Figures S6K–S6S), respectively, indicative of heterogeneity even within this circumscribed population of CeS neurons.

In summary, these results suggest that CeS neurons may simultaneously access spinal motor circuits through direct inputs to spinal interneurons and indirect relays via descending neurons in the brain to exert nuanced control over motor output.

DISCUSSION

Motor areas in the brain need to ultimately act through pre-motor and motor networks in the brainstem and the spinal cord to enable movement. Thus, by unraveling how motor centers in the brain are organized with respect to spinal centers that execute movement, we may gain fundamental understanding of the functional logic of motor networks. We took advantage of virus-based intersectional genetic techniques to define the organization and function of CeS neurons, a poorly understood, circumscribed population of neurons in the DCN with direct inputs to the spinal cord. Specifically, we (1) identified distinct sub-populations of neurons in the DCN based on their patterns of connectivity with the spinal cord, (2) functionally dissected the contribution of anatomically distinct populations of pre-cervical CeS neurons to skilled motor performance and learning, and (3) delineated direct and indirect neuronal relays through which the cerebellum may mediate the coordination of multiple spinal cord segments.

How are cerebellar circuits organized to precisely control different parts of the body and exert their role in motor coordination? There is significant evidence for broad topography in the arrangement of inputs from the cerebellar cortex to the DCN and also functional somatotopy within the DCN and their connections with the motor thalamus and the red nucleus (Courville, 1966; Middleton and Strick, 2001). However, it is not clear how the topography of the DCN is transformed into control over spinal cord circuits for specific body regions. Here, we found that a small minority of neurons in the interpositus and fastigial nuclei display highly specific patterns of connectivity with different segments of the spinal cord. There were clear distinctions in the organization of the DCN with respect to the right and left halves of the cervical, thoracic, and lumbar segments of the spinal cord. While the IntP and fastigial nuclei contained only pre-cervical neurons, the IntA contained pre-cervical, pre-lumbar, and prethoracic neurons. Within the IntA, pre-cervical and pre-lumbar neurons were non-overlapping and occupied distinct domains chiefly along the mediolateral axis of the nucleus. This arrangement roughly corresponds to that of the "forelimb" and "hindlimb" areas of the IntA nucleus (Garwicz and Ekerot, 1994), which were designated based on inputs from cerebellar micro-zones and receptive field mapping. Together, these

results support the idea of a modular organization of the IntA nucleus (Apps and Garwicz, 2005; Garwicz and Ekerot, 1994), where each body part is discretely represented within the nucleus and is reminiscent of the organization of corticospinal neurons and rubrospinal neurons, which are stratified in their resident motor areas based on inputs to the cervical and lumbar segments of the spinal cord.

A modular organization of the IntA may offer specialized control over each major body segment, such as dexterous hand control during voluntary forelimb movement. This idea is supported by observations of a loss of skilled movements of the ipsilateral limb upon damage to the interpositus (Becker and Person, 2019; Chambers and Sprague, 1955; Cooper et al., 2000; Konczak et al., 2010; Low et al., 2018; Martin et al., 2000; Milak et al., 1997; Uno et al., 1973; Zackowski et al., 2002). This prompted us to test whether CeS[cer-ipsi] neurons, which are enriched in the IntA nucleus, represent a critical cellular component of these nuclei in skilled forelimb control. Indeed, we found a continuous requirement for these neurons in executing skilled forelimb movement in the single-pellet retrieval task. Additionally, two features of movement were reminiscent of the deficits seen in patients with acute cerebellar damage (Holmes, 1917; Konczak et al., 2010; Zackowski et al., 2002) and experimental models of IntA silencing (Cooper et al., 2000; Martin et al., 2000; Milak et al., 1997; Uno et al., 1973). First, upon CeS[cer-ipsi] silencing, mice took longer to establish contact with the pellet. This may be similar to clinical bradykinesia and could stem from a loss of predictive control and greater reliance on slow sensory feedback to guide the arm (Wolpert et al., 1998) and/or the inability to exert corrective action upon predicting deviation in the desired path. On the other hand, it may also be a compensatory mechanism similar to that seen in patients with cerebellar damage, wherein movements are decomposed to favor accuracy (Zackowski et al., 2002). Second, upon CeS[cer-ipsi] silencing, mice failed to grasp the pellet despite extending their digits and instead dislodged the pellet. This could reflect the inability to predict or implement proper grip aperture and/or the inability to couple reach and grasp movements to achieve endpoint precision (Jeannerod, 1984).

During normal behavior, the cerebellum cooperates with other brain regions to produce coordinated movements, and it is likely that CeS[cer-ipsi] neurons similarly work in concert with other descending pathways to regulate spinal circuits. Interestingly, the effects that we observed upon silencing CeS[cer-ipsi] neurons were distinct from those of acutely inhibiting three other main sources of descending neurons that are known to be involved in dexterous forelimb control: the motor cortex, red nucleus, and medullary ventral (MdV) reticular formation. Ablation or silencing of corticospinal neurons perturbs multiple phases of skilled pellet retrieval (Ueno et al., 2018; Wang et al., 2017), while silencing the broader motor cortex blocks ongoing forelimb movements (Guo et al., 2015). Lesion of the red nucleus does not affect the reach component of the task, but it results in a faster grasp and defects in the arpeggio movements of the digits (Morris et al., 2015; Rizzi et al., 2019; Sybirska and Górska, 1980; Whishaw and Gorny, 1996). Similarly, silencing the MdV also impairs the grasp phase of pellet retrieval (Esposito et al., 2014). Thus, although CeS neurons represent only 1%–2% of all descending neurons targeting the spinal cord (Liang et al., 2011), CeS[cer-ipsi] neurons have a unique role in skilled reaching that cannot be compensated through other pathways.

CeS neurons in the fastigial and IntP nuclei predominantly project to the cervical spinal cord, in contrast to those in the IntA. CeS neurons within the fastigial nucleus were found throughout the nucleus and specifically targeted the contralateral cervical spinal cord. Within the IntP, CeS neurons may be further fractionated into two populations based on target and anatomy: ipsilateral IntP CeS neurons that were diffusely distributed throughout the nucleus and contralaterally projecting neurons that tended to be located closer to the midline. Notably, the medial portion of the IntP receives input from the X and CX zones of the cerebellar cortex, as opposed to greater C2 input into the rest of the IntP (Buisseret-Delmas et al., 1993). Additionally, our observation that medially located IntP neurons project to the contralateral cervical spinal cord, together with the somatotopic organization of CeS^cer-ipsi and CeS^lum-ipsi IntA neurons, suggests that the highly refined olivo-cortico-nuclear circuitry (Jansen and Brodal, 1940; Oscarsson and Uddenberg, 1966; Voogd and Koehler, 2018) may be extended to the outputs of DCN neurons.

By manipulating CeS^cer-contra neurons, we found a specific requirement for these cells in the skilled locomotor rotarod task in which animals need to learn to adapt their motor output to stay on an accelerating rod (Buitrago et al., 2004; Dunham and Miya, 1957). It is known that the broader fastigial nucleus is the site of the "cerebellar locomotor region," which, when stimulated, can drive locomotion (Mori et al., 1999, 2000) and, when ablated, results in ataxia and defects in interlimb coordination (Chambers and Sprague, 1955; Yu and Eidelberg, 1983). However, the fastigial and IntP contain only pre-cervical neurons, which raised the question of how these neurons fulfill the roles of their broader nuclei in locomotor stability and coordination.

We found that these CeS^cer-contra neurons contacted a diverse set of synaptic targets that, together, could serve as substrates for binding the activity of descending neurons in the brain with that of segmental and long-range neurons in the spinal cord. This in turn could allow CeS^cer-contra neurons to orchestrate the output of multiple motor segments to bring about coordinated movements. First, CeS^cer-contra neurons targeted En1+ neurons within the cervical spinal cord, which controls the neck and forelimbs. These are segmental, inhibitory, pre-motor neurons, which are known to regulate the burst duration of local motoneurons (Bikoff et al., 2016; Falgairolle and O'Donovan, 2019; Gosgnach et al., 2006; Wenner and O'Donovan, 1999). Second, CeS^cer-contra neurons targeted LDP neurons in the cervical cord, which synapse onto pre-motor networks and motoneurons in the thoracic and lumbar regions and thus exert control over the trunk and hindlimb, respectively (Flynn et al., 2017; Miller and van der Burg, 1973; Ni et al., 2014; Ruder et al., 2016; Sherrington and Laslett, 1903; Skinner et al., 1979). Thus, CeS^cer-contra neurons may recruit spinal neurons as ensembles to coordinate the output of multiple spinal segments. Third, we observed extensive collateralization of CeS neurons in the brain. With the exception of the pontine TRN, the cerebellar cortex, and the thalamus, most of the observed targets of CeS^cer-contra neurons in the brain are important sources of descending pathways. The collateralization pattern of CeS^cer-contra neurons is in accord with the proposal that the cerebellum may enable coordinated movement by accurately timing the output of descending pathways, which was based on observations of a loss of rhythmicity in descending neurons during locomotion in decerebellated animals (Arshavsky et al., 1983; Orlovsky, 1972a, 1972b; Shik and Orlovsky, 1976). Given that some CeS^cer-contra neurons can simultaneously target multiple descending

pathways and the spinal cord, we propose that the cerebellum brings about coordinated motor outputs by orchestrating the activity of other descending pathways together with that of its direct spinal targets.

Notably, manipulating CeS[cer-contra] neurons did not produce overt defects in normal locomotion, balance, or the execution of skilled locomotion once motor learning had occurred. This is in contrast with the other descending pathways and may reflect the fact that each of these descending pathways synapses onto a unique complement of functionally diverse spinal neurons. CeS[cer-contra] neurons terminate principally in lamina VIII of the cervical spinal cord, the hub of interlimb coordination (Jankowska, 1992; Watson et al., 2009). This termination zone partly overlaps with that of the vestibulospinal and reticulospinal pathways. Vestibulospinal neurons from the lateral vestibular nucleus also terminate in lamina IX, where they directly synapse onto ipsilateral extensor motoneurons, and to a lesser extent in laminae VII and VIII (Basaldella et al., 2015; Grillner et al., 1970; Liang et al., 2014; Murray et al., 2018). Accordingly, stimulating the vestibulospinal pathway provokes extensor activity to support balance, and ablation of these neurons leads to overt deficits in balance and locomotion (Orlovsky, 1972c; Yu and Eidelberg, 1981). The reticulospinal pathway originates in various discrete nuclei in the brainstem and targets the ventral horn broadly, including extensor and flexor motoneurons (Esposito et al., 2014; Liang et al., 2016; Watson et al., 2009), and plays diverse roles in motor control. The rubrospinal pathway targets laminae IV–VI in the contralateral spinal cord (Liang et al., 2012), where reflex encoders (Schouenborg et al., 1995), motor synergy encoders (Levine et al., 2014), and other populations involved in sensorimotor integration reside. While the red nucleus is known to be rhythmically active during locomotion (Orlovsky, 1972a), its role in skilled locomotor learning in unclear. Nevertheless, ablation of the red nucleus impairs the ability to control distal joints in the forelimb and hindlimb (Rizzi et al., 2019; Shik et al., 1966). Finally, the corticospinal tract targets both the deep dorsal horn and the ventral horn of the spinal cord. While broad interventions that target the primary or secondary motor cortex perturb rotarod locomotion, a specific role for corticospinal neurons in basic or skilled locomotion is not clear (Cao et al., 2015; DiGiovanna et al., 2016; Farr et al., 2006; Hayashi-Takagi et al., 2015; Miri et al., 2017). Together, the requirement for CeS[cer-contra] neurons in skilled locomotor learning is distinct from the functions of other descending neurons and may reflect the complementary roles played by different descending pathways and their corresponding motor areas in mediating the learning and execution of skilled locomotion.

How may CeS[cer-contra] neurons participate in motor learning? One possibility is that these neurons, which are known to receive multimodal sensory input and cerebellar input (Eccles et al., 1974; Wilson et al., 1978), may modulate the responsiveness of their spinal targets to other descending and sensory input (Matsuyama and Jankowska, 2004; Wilson et al., 1978) during the learning phase of the task, in a manner that allows sensorimotor adaptation. This possibility is supported by the following reports. First, it has been shown that individual LDP neurons receive convergent input from multiple descending pathways, including the fastigial nucleus (Alstermark et al., 1987). Second, there is evidence for temporal facilitation of post-synaptic potentials in spinal neurons following stimulation of the cerebellar commissure and the ipsilateral lateral vestibular nucleus or reticulospinal pathways

(Matsuyama and Jankowska, 2004). Alternatively, the site of synaptic plasticity may be in the cerebellum. For example, neurons in the interpositus and fastigial nuclei have recently been shown to participate in motor adaptation (Brooks et al., 2015; Darmohray et al., 2019). Lastly, CeS neurons may work in concert with the motor cortex through relays in the thalamus to enable motor learning (Ito, 1984).

Together, this suggests that there are dual modes through which CeS$^{cer-contra}$ neurons can influence spinal output: (1) directly through its spinal targets and (2) through descending neurons in the brain. However, it is unlikely that the dual paths from these neurons are functionally redundant because each of these descending pathways synapses onto a unique complement of functionally diverse spinal neurons; far from being passive relays, they perform unique integrative functions and thereby serve as anatomical substrates for the differential contributions of each of the descending pathways to motor control. Moreover, the extensive collateralization of CeS neurons is reminiscent of other descending pathways (Akintunde and Buxton, 1992; Beitzel et al., 2017; Brodal and Gogstad, 1954; Economo et al., 2018; Wang et al., 2018; Wiesendanger, 1969) and may serve several important functions: (1) to provide internal copies of motor commands to update the collateral targets of the current status of the effector (Sperry, 1950); (2) to coordinate the output of the rubrospinal, vestibulospinal, and reticulospinal neurons, and spinal neurons to bring about complex patterns of sequential muscle contractions (Shik and Orlovsky, 1976); or (3) to facilitate or gate the responsiveness of descending pathways and spinal neurons to incoming sensory input (Brooks et al., 2015; Orlovsky and Pavlova, 1972) and that of shared spinal targets to convergent descending inputs (Matsuyama and Jankowska, 2004). These dual paths from CeS$^{cer-contra}$ neurons could serve to provide a broad range of synergistic control over spinal output. However, one of the technical implications of this extensive pattern of collateralization for any descending pathway is that it is currently difficult to ascribe the behavioral phenotype specifically to the spinal axonal branch of descending neurons without differentially silencing the axons in the spinal cord. Future advances in genetic techniques may facilitate experiments to dissect the behavioral role of each of these pathways at the synaptic level.

Overall, this study establishes a contemporary foundation for our knowledge of CeS neurons and is an important step toward the goal of understanding how various regions of the central nervous system function together to mediate voluntary movement and behavior.

STAR★METHODS

RESOURCE AVAILABILITY

Lead Contact—Further information and requests for resources and reagents should be directed to and will be fulfilled by the Lead Contact, Ariel J Levine (ariel.levine@nih.gov).

Materials Availability—All unique/stable reagents generated in this study are available from the Lead Contact with a completed Materials Transfer Agreement.

Data and Code Availability—This study did not generate any unique datasets or code.

EXPERIMENTAL MODEL AND SUBJECT DETAILS

Mice—All animal experiments were performed in accordance with institutional guidelines and approved (protocol#1384) by the National Institute of Neurological Disorder and Stroke's Institutional Animal Care and Use Committee. All mouse lines were maintained on a mixed background of C57BL/6J and BALB/cJ and were housed on a 12hr/12hr light dark cycle with standard chow. In addition to wild-type mice, the following strains were used: Ai14 tdTomato reporter mice (B6.Cg-GT(ROSA)26Sor$^{tm14(CAG-tdTomato)HZe}$/J) (Madisen et al., 2010), En1-Cre (Kimmel et al., 2000) (En1$^{tm2(cre)/Wrst}$/J mice), and ChAT-Cre (B6;129S6-Chat$^{(tm1cre)Lowl}$/J) (Rossi et al., 2011). Approximately equal numbers of male and female mice between 3–20 weeks of age were used for all experiments.

Viruses—AAV viruses were produced at Vigene Biosciences or were purchased from the UNC Viral Vector Core and Addgene. Plasmids for each AAV were either produced in-house using pAAV-hSyn-DIO-hM4Di-mCherry as a backbone (Krashes et al., 2011), or were obtained from Addgene (Krashes et al., 2011; Madisen et al., 2015; Xue et al., 2014). Viral particles were injected at a titer of 1–5^{E12} genome copies per ml.

METHOD DETAILS

Surgery for spinal cord and cerebellar injections—Mice were anesthetized by intraperitoneal injection of a drug cocktail containing fentanyl (0.2 mg.kg), dexmedetomidin (1 mg/kg), and midazolam (5 mg/kg) dissolved in saline. For spinal injections, a small incision was made in the skin and the underlying musculature or adipose tissue was teased apart to reveal the vertebral column. Tissue joining the dorsal processes of consecutive vertebrae was removed and the vertebral surfaces were cleaned with fine forceps and gently separated (for lumbar injections) to reveal the dorsal surface of the spinal cord. The dura was punctured by pinching with sharp forceps to facilitate smooth entry of the needle. Virus was pressure injected through a pulled glass needle at a depth of 700–800 μm from the dorsal surface and 250 nL of viral particles was released at a rate of 100 nl/min. Craniotomies were made above the corresponding target areas (coordinates for ipsilateral cerebellar nuclei are AP:−5.88, ML:−1.65, DV:3.37; coordinates for contralateral cerebellar nuclei are AP:−6.12, ML:1.57, DV:3.26; coordinates for thalamus are −2.18; −1.81; 3.45; coordinates for red nucleus are AP:- −3.52; −0.58; 3.75; coordinates for medulla are AP: −6.12; −1.37; 4.15) and viral particles were released at a rate of 100 nl/min, ~150 nL per site. Following injections, the overlying muscle was sutured, and the skin incision was closed using wound clip. Anesthesia was reversed by intraperitoneal administration of buprenorphine (0.1 mg/kg), atipemazole (2.5 mg/kg), and flumenazil (0.2 mg/kg) in saline. Additionally, mice received intradermal injection of meloxicam SR for analgesia and were returned to their home cages.

Histology, immunofluorescence, and *in situ* hybridization—Anesthetized mice were transcardially perfused with PBS followed by cold 4% paraformaldehyde (PFA). Spinal cords and brains were harvested and post-fixed in cold 4% PFA overnight at 4°C, cryoprotected by immersion in 30% sucrose overnight at 4°C, embedded in OCT medium, and sliced into 20 μm (for *in situ* hybridization) or 35–50 μm (for immunofluorescence) sections in a cryostat. For immunofluorescence, transverse spinal sections were directly

mounted onto glass slides or floated in PBS, washed in PBS, blocked in blocking solution (PBS containing 0.3% Triton X-100, 1% bovine serum albumin (BSA), and 4% normal donkey serum), and incubated in primary antibodies, which were diluted in blocking solution at the following concentrations: NeuN (1:500), PSD95 (1:500), and EBFP/GFP (1:500), and CHX10 (1:500), for 24–48 hours. Sections were then washed, incubated with secondary antibodies and fluorescent Nissl stain (1:1000, Neurotrace, Thermofisher, N21483/N21479) for 1–2 hours and mounted. Cerebellar sections (coronal) were washed once in OCT, incubated in PBS containing 0.1% triton and fluorescent Nissl stain (1:2000) for 12–24 hours, and mounted onto slides. For *in situ* hybridization, RNAscope Fluorescent Multiplex Reagent Kit (ACD) was used according to the manufacturer's instructions. Sections were imaged using a Zeiss LSM 800 confocal microscope and processed (tiles were stitched using "stitch tile" function; slices were Z-projected using "orthogonal projection" function) using FIJI (NIH image) and/or Zen2 (Zeiss) software. All images shown are tiled and/or projected z stacks unless otherwise indicated.

Behavioral analysis—Behavior experiments were performed between 4 – 10 weeks following surgery. The experimenter was not blinded to the treatment group. Mice that expressed hM4Di were given saline or CNO (3–5 mg/kg, dissolved in DMSO/saline via intraperitoneal injections) 30 −35 minutes prior to testing. Mice that expressed KORD were given DMSO or salvinorin (10 mg/kg, dissolved in DMSO via subcutaneous injections) 15 minutes prior to testing.

<u>Single pellet reaching task:</u> Mice were food restricted to 85%–90% of their body weight for four days leading up to the test and throughout the entire duration of the test. On days 3 and 4 following food restriction, chocolate pellets were placed on the cage floor to familiarize the mice with these pellets. Four days following food restriction, mice were habituated to the test chamber (plexiglass box, 1'[l]x1'[h]x0.5′[w] with an 8 mm wide slot) for 15 minutes. A chocolate pellet was placed on pedestal (height 5 mm), which was placed outside the box, at a perpendicular distance of 8mm from the right edge of the slot. Mice were then motivated to use their left paw (paw corresponding to the injected side) to retrieve the pellet. Once the mice made 5 consecutive attempts to reach for the pellet, they were given at least 20 trials on days 1 and 2 and were given 40 trials on subsequent days. Each trial was scored as a success or a failure according to the following definitions. A trial was scored as success when the mouse was able to retrieve the pellet and place it in its mouth (Video S1). Failed trials were classified into three groups based on the nature of the error - failure to guide arm to the pellet; 'dislodging the pellet' in which the mouse touches the pellet but knocks it off the pedestal or fails to grasp the pellet; dropping of retrieved pellet (Video S1). Mice were excluded from the task if they failed to attempt to reach for pellets within 3 days of training or if they preferred using the tongue or the paw corresponding to the uninjected side. On day 10, the trials were videotaped at 240 frames per second and the duration of the three main phases of the task was calculated from trials where the mouse made a single fluid attempt to retrieve the pellet ($> 80\%$ of all trials). Phase 1: time from lift off to establishing contact with the pellet (for successful or dropped trials) or dislodging the pellet (for failed trials), phase2: time spent to grasp the pellet (only successful trials and

dropped trials), phase 3: time from lifting pellet to putting it in the mouth (only successful trials).

Open-field analysis: Mice were placed in an open field (Cleversys, Inc.) and the first five minutes of their activity (distance traveled and velocity) was recorded and analyzed using manufacturer supplied software.

Gait analysis: Mice were forced to run on a motorized treadmill belt (Cleversys, Inc.) at a constant speed of 20 cm per second for 20 s with and without CNO. Videos were captured at a rate of 80 frames per second. Seven to eleven consecutive steps were analyzed for each mouse using manufacturer supplied software.

Rotarod analysis: Mice were habituated to the rotarod apparatus (Panlab, Harvard apparatus) a day prior to the test. During this period, mice were placed on a rotarod rotating at 4 rpm for a maximum of five minutes. On subsequent days, mice were treated with either vehicle or ligand (CNO or Salvinorin B) and the latency to fall from the accelerating rotarod (4 – 40 rpm over 5 minutes) was measured. The mice were given 4 trials a day for four days. Mice were excluded from the task if they failed to stay on the rotarod for longer than 30 s on the day of habituation or if they intentionally jumped off the rod on subsequent days.

Beam walk analysis: Mice were trained to cross two beams (1 m long) of different widths (wide beam: 12 mm; narrow beam: 6mm). Two- and four-days following training, mice were tested with vehicle and CNO, respectively. Videos were captured at a rate of 120 frames per second and the time taken to cross a 0.7 m section of the beam was measured. Mice were given a maximum of six trials and only trials that did not involve any stalling were analyzed.

Exclusion criteria: Twenty-seven percent of injected mice were excluded before from behavioral analysis due to apparent abnormalities of the limb corresponding to the injected side of the spinal cord. For viral injections, the brain and spinal cord of every experimental animal was examined post hoc to ensure that viral expression was present and was accurately and specifically targeted to the desired location while maintaining normal tissue morphology. Approximately 20% of animals were excluded due to inaccurate injections of the deep cerebellar nuclei that spread to the nearby vestibular nuclei or due to disrupted morphology. Assay-specific exclusion criteria are described above.

QUANTIFICATION AND STATISTICAL ANALYSIS

Behavioral statistical testing—Two-way ANOVA (repeated-measures) was used for multi-day testing behaviors (reaching and rotarod) and two-tailed t tests (paired or unpaired) were used all for all other behavioral analysis, as indicated in figure legends. Differences among groups were considered significant if $p < 0.05$. P values are denoted by asterisks: *$p < 0.05$; **$p < 0.01$; ***$p < 0.001$; ****$p < 0.0001$; n.s – not significant. Data are represented as mean ± SEM unless otherwise indicated. Statistical analyses were performed using GraphPad prism software.

Cellular target quantification—Laminar borders were determined based on an established adult mouse spinal cord atlas (Watson et al., 2009). Synaptic contacts onto

candidate target cells were counted in 20X single optical sections. Serial optical sections (1.16 μm) over a depth of 35 μm were collected using a 20X lens and determination of presence or absence of synaptic input (apposition of synaptophysin EGFP and PSD95) was made by analyzing single optical sections. For each candidate target cell type, quantification was done using at least four sections per spinal cord and at least three independent spinal cord samples.

Estimation of co-infection efficiency of AAVretro-H2B-GFP and AAVretro-H2B-mCherry—The above viruses were co-injected into the spinal cord. Quantification of the total number of GFP+ neurons, mCherry+ neurons, and double-positive neurons revealed 80% co-localization efficiency (percentage of double positive neurons: 81.4 ± 1.7%, mean ± SEM, n = 3 mice). Results from collateralization estimation experiments in Figures S6K–S6S need to be interpreted within the context of this experiment and collateralization estimation could be an underestimation of percentage of CeS neurons with collaterals to the respective targets.

Deep cerebellar neuron quantification—Deep cerebellar nuclei were delineated in coronal sections stained with fluorescent Nissl stain based on an established brain atlas () (Paxinos and Franklin, 2007). For quantification of total number of neurons, only 'large' neurons with conspicuous cytoplasm around the nucleus (diameter > 10 μm) (Heckroth, 1994) were counted.

Density plot of synaptic terminals—For each level of the spinal cord, an image each was collected of sections from the same level from three different animals. The images were aligned using the central canal as an anchor and stacked together using the z-project function in FIJI. The individual channels were separated (NeuN - blue, synaptophysin - green) and signal from either channel was thresholded and filtered based on mean particle density. Using the Look-Up Table (LUT) function, a 'fire' color gradient was assigned to each image.

Supplementary Material

Refer to Web version on PubMed Central for supplementary material.

ACKNOWLEDGMENTS

REFERENCES

Akintunde A, and Buxton DF (1992). Quadruple labeling of brain-stem neurons: a multiple retrograde fluorescent tracer study of axonal collateralization.J. Neurosci. Methods 45, 15–22. [PubMed: 1283430]

Alstermark B, Lundberg A, Pinter M, and Sasaki S (1987). Long C3-C5 propriospinal neurones in the cat. Brain Res. 404, 382–388. [PubMed: 3032341]

Ampatzis K, Song J, Ausborn J, and El Manira A (2014). Separate micro-circuit modules of distinct v2a interneurons and motoneurons control the speed of locomotion. Neuron 83, 934–943. [PubMed: 25123308]

Angaut P, and Bowsher D (1965). Cerebello-rubral connexions in the cat. Nature 208, 1002–1003. [PubMed: 5868843]

Apps R, and Garwicz M (2005). Anatomical and physiological foundations of cerebellar information processing. Nat. Rev. Neurosci 6, 297–311. [PubMed: 15803161]

Armstrong DM (1986). Supraspinal contributions to the initiation and control of locomotion in the cat. Prog. Neurobiol 26, 273–361. [PubMed: 3526411]

Arshavsky YI, Gelfand IM, and Orlovsky GN (1983). The cerebellum and control of rhythmical movements. Trends Neurosci. 6, 417–422.

Asanuma C, Thach WT, and Jones EG (1980). Nucleus interpositus projection to spinal interneurons in monkeys. Brain Res. 191, 245–248. [PubMed: 6769539]

Asanuma C, Thach WT, and Jones EG (1983). Distribution of cerebellar terminations and their relation to other afferent terminations in the ventral lateral thalamic region of the monkey. Brain Res. 286, 237–265. [PubMed: 6189561]

Bagnall MW, Zingg B, Sakatos A, Moghadam SH, Zeilhofer HU, and du Lac S (2009). Glycinergic projection neurons of the cerebellum.J. Neurosci 29, 10104–10110. [PubMed: 19675244]

Barker LF (1901). The Nervous system and its constituent neurons. J. Am. Med. Assoc 33, 1307.

Basaldella E, Takeoka A, Sigrist M, and Arber S (2015). Multisensory Signaling Shapes Vestibulo-Motor Circuit Specificity. Cell 163, 301–312. [PubMed: 26451482]

Batton RR 3rd, Jayaraman A, Ruggiero D, and Carpenter MB (1977). Fastigial efferent projections in the monkey: an autoradiographic study.J. Comp. Neurol 174, 281–305. [PubMed: 68041]

Becker MI, and Person AL (2019). Cerebellar Control of Reach Kinematics for Endpoint Precision. Neuron 103, 335–348.e5. [PubMed: 31174960]

Beitzel CS, Houck BD, Lewis SM, and Person AL (2017). Rubrocerebellar Feedback Loop Isolates the Interposed Nucleus as an Independent Processor of Corollary Discharge Information in Mice. J. Neurosci 37, 10085–10096. [PubMed: 28916520]

Bikoff JB, Gabitto MI, Rivard AF, Drobac E, Machado TA, Miri A, Brenner-Morton S, Famojure E, Diaz C, Alvarez FJ, et al. (2016). Spinal Inhibitory Interneuron Diversity Delineates Variant Motor Microcircuits. Cell 165, 207–219. [PubMed: 26949184]

Briscoe J, Pierani A, Jessell TM, and Ericson J (2000). A homeodomain protein code specifies progenitor cell identity and neuronal fate in the ventral neural tube. Cell 101, 435–445. [PubMed: 10830170]

Brodal A, and Gogstad AC (1954). Rubro-cerebellar connections; an experimental study in the cat. Anat. Rec 118, 455–485. [PubMed: 13158865]

Brodal A, and Szikla G (1972). The termination of the brachium conjunctivum descendens in the nucleus reticularis tegmenti pontis. An experimental anatomical study in the cat. Brain Res. 39, 337–351. [PubMed: 4113021]

Brooks JX, Carriot J, and Cullen KE (2015). Learning to expect the unexpected: rapid updating in primate cerebellum during voluntary self-motion. Nat. Neurosci 18, 1310–1317. [PubMed: 26237366]

Buisseret-Delmas C, Yatim N, Buisseret P, and Angaut P (1993). The X zone and CX subzone of the cerebellum in the rat. Neurosci. Res 16, 195–207. [PubMed: 7683779]

Buitrago MM, Schulz JB, Dichgans J, and Luft AR (2004). Short and long-term motor skill learning in an accelerated rotarod training paradigm. Neurobiol. Learn. Mem 81, 211–216. [PubMed: 15082022]

Cajal SRY (2012). Texture of the Nervous System of Man and the Vertebrates (Springer Science & Business Media).

Canto CB, Witter L, and De Zeeuw CI (2016). Whole-Cell Properties of Cerebellar Nuclei Neurons In Vivo. PLoS ONE 11, e0165887. [PubMed: 27851801]

Cao VY, Ye Y, Mastwal S, Ren M, Coon M, Liu Q, Costa RM, and Wang KH (2015). Motor Learning Consolidates Arc-Expressing Neuronal Ensembles in Secondary Motor Cortex. Neuron 86, 1385–1392. [PubMed: 26051420]

Carrea RME, and Mettler FA (1947). Physiologic consequences following extensive removals of the cerebellar cortex and deep cerebellar nuclei and effect of secondary cerebral ablations in the primate. J. Comp. Neurol 87, 169–288. [PubMed: 20271577]

Carrea RM, and Mettler FA (1954). The anatomy of the primate brachium conjunctivum and associated structures. J. Comp. Neurol 101, 565–689. [PubMed: 13233356]

Castro AJ (1972). The effects of cortical ablations on digital usage in the rat. Brain Res. 37, 173–185. [PubMed: 5061111]

Chabrol FP, Blot A, and Mrsic-Flogel TD (2019). Cerebellar Contribution to Preparatory Activity in Motor Neocortex. Neuron 103, 506–519.e4. [PubMed: 31201123]

Chambers WW, and Sprague JM (1955). Functional localization in the cerebellum. II. Somatotopic organization in cortex and nuclei. AMA Arch. Neurol. Psychiatry 74, 653–680. [PubMed: 13268132]

Chan-Palay V (2013). Cerebellar Dentate Nucleus (Springer).

Clarke RH, and Horsley V (1905). On the intrinsic fibres of the cerebellum, its nuclei and its efferent tracts. Brain 28, 13–29.

Cooper SE, Martin JH, and Ghez C (2000). Effects of inactivation of the anterior interpositus nucleus on the kinematic and dynamic control of multijoint movement. J. Neurophysiol 84, 1988–2000. [PubMed: 11024092]

Courville J (1966). Somatotopical organization of the projection from the nucleus interpositus anterior of the cerebellum to the red nucleus. An experimental study in the cat with silver impregnation methods. Exp. Brain Res 2, 191–215. [PubMed: 4163693]

Crone SA, Zhong G, Harris-Warrick R, and Sharma K (2009). In mice lacking V2a interneurons, gait depends on speed of locomotion. J. Neurosci 29, 7098–7109. [PubMed: 19474336]

Darmohray DM, Jacobs JR, Marques HG, and Carey MR (2019). Spatial and Temporal Locomotor Learning in Mouse Cerebellum. Neuron 102, 217–231.e4. [PubMed: 30795901]

De Zeeuw CI, Simpson JI, Hoogenraad CC, Galjart N, Koekkoek SK, and Ruigrok TJ (1998). Microcircuitry and function of the inferior olive. Trends Neurosci. 21, 391–400. [PubMed: 9735947]

DiGiovanna J, Dominici N, Friedli L, Rigosa J, Duis S, Kreider J, Beauparlant J, van den Brand R, Schieppati M, Micera S, and Courtine G (2016). Engagement of the Rat Hindlimb Motor Cortex across Natural Locomotor Behaviors. J. Neurosci 36, 10440–10455. [PubMed: 27707977]

Dunham NW, and Miya TS (1957). A note on a simple apparatus for detecting neurological deficit in rats and mice. J. Am. Pharm. Assoc. Am. Pharm. Assoc 46, 208–209. [PubMed: 13502156]

Eccles JC, Sabah NH, and Táboríková H (1974). The pathways responsible for excitation and inhibition of fastigial neurones. Exp. Brain Res 19, 78–99. [PubMed: 4360384]

Economo MN, Viswanathan S, Tasic B, Bas E, Winnubst J, Menon V, Graybuck LT, Nguyen TN, Smith KA, Yao Z, et al. (2018). Distinct descending motor cortex pathways and their roles in movement. Nature 563, 79–84. [PubMed: 30382200]

Esposito MS, Capelli P, and Arber S (2014). Brainstem nucleus MdV mediates skilled forelimb motor tasks. Nature 508, 351–356. [PubMed: 24487621]

Falgairolle M, and O'Donovan MJ (2019). V1 interneurons regulate the pattern and frequency of locomotor-like activity in the neonatal mouse spinal cord. PLoS Biol. 17, e3000447. [PubMed: 31513565]

Farr TD, Liu L, Colwell KL, Whishaw IQ, and Metz GA (2006). Bilateral alteration in stepping pattern after unilateral motor cortex injury: a new test strategy for analysis of skilled limb movements in neurological mouse models. J. Neurosci. Methods 153, 104–113. [PubMed: 16309746]

Flynn JR, Conn VL, Boyle KA, Hughes DI, Watanabe M, Velasquez T, Goulding MD, Callister RJ, and Graham BA (2017). Anatomical and Molecular Properties of Long Descending Propriospinal Neurons in Mice. Front. Neuroanat 11, 5. [PubMed: 28220062]

Friese A, Kaltschmidt JA, Ladle DR, Sigrist M, Jessell TM, and Arber S (2009). Gamma and alpha motor neurons distinguished by expression of transcription factor Err3. Proc. Natl. Acad. Sci. USA 106, 13588–13593. [PubMed: 19651609]

Fukushima K, Peterson BW, Uchino Y, Coulter JD, and Wilson VJ (1977). Direct fastigiospinal fibers in the cat. Brain Res. 126, 538–542. [PubMed: 861735]

Garwicz M, and Ekerot CF (1994). Topographical organization of the cerebellar cortical projection to nucleus interpositus anterior in the cat. J. Physiol 474, 245–260. [PubMed: 8006811]

Gosgnach S, Lanuza GM, Butt SJB, Saueressig H, Zhang Y, Velasquez T, Riethmacher D, Callaway EM, Kiehn O, and Goulding M (2006). V1 spinal neurons regulate the speed of vertebrate locomotor outputs. Nature 440, 215–219. [PubMed: 16525473]

Gray H (1918). Anatomy of the Human Body (Lea & Febiger).

Gray LP (1926). Some experimental evidence on the connections of the vestibular mechanism in the cat. J. Comp. Neurol 41, 319–364.

Grillner S, Hongo T, and Lund S (1970). The vestibulospinal tract. Effects on alpha-motoneurones in the lumbosacral spinal cord in the cat. Exp. Brain Res 10, 94–120. [PubMed: 5411977]

Guo J-Z, Graves AR, Guo WW, Zheng J, Lee A, Rodríguez-González J, Li N, Macklin JJ, Phillips JW, Mensh BD, et al. (2015). Cortex commands the performance of skilled movement. eLife 4, e10774. [PubMed: 26633811]

Hayashi-Takagi A, Yagishita S, Nakamura M, Shirai F, Wu YI, Loshbaugh AL, Kuhlman B, Hahn KM, and Kasai H (2015). Labelling and optical erasure of synaptic memory traces in the motor cortex. Nature 525, 333–338. [PubMed: 26352471]

Heckroth JA (1994). Quantitative morphological analysis of the cerebellar nuclei in normal and lurcher mutant mice. I. Morphology and cell number. J. Comp. Neurol 343, 173–182. [PubMed: 8027434]

Holmes G (1917). The symptoms of acute cerebellar injuries due to gunshot injuries. Brain 40, 461–535.

Ito M (1984). The Cerebellum and Neural Control (Raven Press).

Jakob C (1942). La sistematización del haz central de la calota como vía neoneuronal cerebelosa aferente olivobulbar. Rev. Neurol. Buenos Aires 7, 1–24.

Jankowska E (1992). Interneuronal relay in spinal pathways from proprioceptors. Prog. Neurobiol 38, 335–378. [PubMed: 1315446]

Jansen J, and Brodal A (1940). Experimental studies on the intrinsic fibers of the cerebellum. II. The cortico-nuclear projection. J. Comp. Neurol 73, 267–321.

Jeannerod M (1984). The timing of natural prehension movements. J. Mot. Behav 16, 235–254. [PubMed: 15151851]

Kandel E (2013). Principles of Neural Science, Fifth Edition (McGraw Hill Professional).

Kelly RM, and Strick PL (2003). Cerebellar loops with motor cortex and prefrontal cortex of a nonhuman primate. J. Neurosci 23, 8432–8444. [PubMed: 12968006]

Kimmel RA, Turnbull DH, Blanquet V, Wurst W, Loomis CA, and Joyner AL (2000). Two lineage boundaries coordinate vertebrate apical ectodermal ridge formation. Genes Dev. 14, 1377–1389. [PubMed: 10837030]

Kimura Y, Okamura Y, and Higashijima S (2006). alx, a zebrafish homolog of Chx10, marks ipsilateral descending excitatory interneurons that participate in the regulation of spinal locomotor circuits. J. Neurosci 26, 5684–5697. [PubMed: 16723525]

Konczak J, Pierscianek D, Hirsiger S, Bultmann U, Schoch B, Gizewski ER, Timmann D, Maschke M, and Frings M (2010). Recovery of upper limb function after cerebellar stroke: lesion symptom mapping and arm kinematics. Stroke 41, 2191–2200. [PubMed: 20814010]

Krashes MJ, Koda S, Ye C, Rogan SC, Adams AC, Cusher DS, Maratos-Flier E, Roth BL, and Lowell BB (2011). Rapid, reversible activation of AgRP neurons drives feeding behavior in mice. J. Clin. Invest 121, 1424–1428. [PubMed: 21364278]

Levine AJ, Lewallen KA, and Pfaff SL (2012). Spatial organization of cortical and spinal neurons controlling motor behavior. Curr. Opin. Neurobiol 22, 812–821. [PubMed: 22841417]

Levine AJ, Hinckley CA, Hilde KL, Driscoll SP, Poon TH, Montgomery JM, and Pfaff SL (2014). Identification of a cellular node for motor control pathways. Nat. Neurosci 17, 586–593. [PubMed: 24609464]

Liang H, Paxinos G, and Watson C (2011). Projections from the brain to the spinal cord in the mouse. Brain Struct. Funct 215, 159–186. [PubMed: 20936329]

Liang H, Paxinos G, and Watson C (2012). The red nucleus and the rubrospinal projection in the mouse. Brain Struct. Funct 217, 221–232. [PubMed: 21927901]

Liang H, Bácskai T, Watson C, and Paxinos G (2014). Projections from the lateral vestibular nucleus to the spinal cord in the mouse. Brain Struct. Funct 219, 805–815. [PubMed: 23503971]

Liang H, Watson C, and Paxinos G (2016). Terminations of reticulospinal fibers originating from the gigantocellular reticular formation in the mouse spinal cord. Brain Struct. Funct 221, 1623–1633. [PubMed: 25633472]

Low AYT, Thanawalla AR, Yip AKK, Kim J, Wong KLL, Tantra M, Augustine GJ, and Chen AI (2018). Precision of Discrete and Rhythmic Forelimb Movements Requires a Distinct Neuronal Subpopulation in the Interposed Anterior Nucleus. Cell Rep. 22, 2322–2333. [PubMed: 29490269]

Madisen L, Garner AR, Shimaoka D, Chuong AS, Klapoetke NC, Li L, van der Bourg A, Niino Y, Egolf L, Monetti C, et al. (2015). Transgenic mice for intersectional targeting of neural sensors and effectors with high specificity and performance. Neuron 85, 942–958. [PubMed: 25741722]

Madisen L, Zwingman TA, Sunkin SM, Oh SW, Zariwala HA, Gu H, Ng LL, Palmiter RD, Hawrylycz MJ, Jones AR, Lein ES, and Zeng H (2010). A robust and high-throughput Cre reporting and characterization system for the whole mouse brain. Nat. Neurosci 13, 133–140. [PubMed: 20023653]

Martin JH, Cooper SE, Hacking A, and Ghez C (2000). Differential effects of deep cerebellar nuclei inactivation on reaching and adaptive control. J. Neurophysiol 83, 1886–1899. [PubMed: 10758100]

Mason CR, Miller LE, Baker JF, and Houk JC (1998). Organization of reaching and grasping movements in the primate cerebellar nuclei as revealed by focal muscimol inactivations. J. Neurophysiol 79, 537–554. [PubMed: 9463420]

Matsushita M, and Hosoya Y (1978). The location of spinal projection neurons in the cerebellar nuclei (cerebellospinal tract neurons) of the cat. A study with the horseradish peroxidase technique. Brain Res. 142, 237–248. [PubMed: 630384]

Matsuyama K, and Jankowska E (2004). Coupling between feline cerebellum (fastigial neurons) and motoneurons innervating hindlimb muscles. J. Neurophysiol 91, 1183–1192. [PubMed: 14973325]

Middleton FA, and Strick PL (2001). Cerebellar projections to the prefrontal cortex of the primate. J. Neurosci 21, 700–712. [PubMed: 11160449]

Milak MS, Shimansky Y, Bracha V, and Bloedel JR (1997). Effects of inactivating individual cerebellar nuclei on the performance and retention of an operantly conditioned forelimb movement. J. Neurophysiol 78, 939–959. [PubMed: 9307126]

Miller S, and van der Burg J (1973). The Function of Long Propriospinal Pathways in the Co-Ordination of Quadrupedal Stepping in the Cat. Control of Posture and Locomotion, Advances in Behavioral Biology (Springer), pp. 561–577.

Miri A, Warriner CL, Seely JS, Elsayed GF, Cunningham JP, Church-land MM, and Jessell TM (2017). Behaviorally Selective Engagement of Short-Latency Effector Pathways by Motor Cortex. Neuron 95, 683–696.e11. [PubMed: 28735748]

Mori S, Matsui T, Kuze B, Asanome M, Nakajima K, and Matsuyama K (1999). Stimulation of a restricted region in the midline cerebellar white matter evokes coordinated quadrupedal locomotion in the decerebrate cat. J. Neurophysiol 82, 290–300. [PubMed: 10400958]

Mori S, Matsui T, Mori F, Nakajima K, and Matsuyama K (2000). Instigation and control of treadmill locomotion in high decerebrate cats by stimulation of the hook bundle of Russell in the cerebellum. Can. J. Physiol. Pharmacol 78, 945–957. [PubMed: 11100943]

Morris R, Vallester KK, Newton SS, Kearsley AP, and Whishaw IQ (2015). The differential contributions of the parvocellular and the magnocellular subdivisions of the red nucleus to skilled reaching in the rat. Neuroscience 295, 48–57. [PubMed: 25813707]

Murray AJ, Croce K, Belton T, Akay T, and Jessell TM (2018). Balance Control Mediated by Vestibular Circuits Directing Limb Extension or Antagonist Muscle Co-activation. Cell Rep. 22, 1325–1338. [PubMed: 29386118]

Ni Y, Nawabi H, Liu X, Yang L, Miyamichi K, Tedeschi A, Xu B, Wall NR, Callaway EM, and He Z (2014). Characterization of long descending premotor propriospinal neurons in the spinal cord. J. Neurosci 34, 9404–9417. [PubMed: 25009272]

Nudo RJ, and Masterton RB (1988). Descending pathways to the spinal cord: a comparative study of 22 mammals. J. Comp. Neurol 277, 53–79. [PubMed: 3198796]

Orioli FL (1961). Descending limb of brachium conjunctivum in cat. An electrophysiological study. J. Neurophysiol 24, 583–594. [PubMed: 14482236]

Orlovsky GN (1972a). Activity of rubrospinal neurons during locomotion. Brain Res. 46, 99–112. [PubMed: 4635376]

Orlovsky GN (1972b). Activity of vestibulospinal neurons during locomotion. Brain Res. 46, 85–98. [PubMed: 4635375]

Orlovsky GN (1972c). The effect of different descending systems on flexor and extensor activity during locomotion. Brain Res. 40, 359–371. [PubMed: 5027169]

Orlovsky GN, and Pavlova GA (1972). Response of Deiters' neurons to tilt during locomotion. Brain Res. 42, 212–214. [PubMed: 5047189]

Oscarsson O, and Uddenberg N (1966). Somatotopic termination of spinoolivocerebellar path. Brain Res. 3, 204–207. [PubMed: 5971524]

Paxinos G, and Franklin KBJ (2007). The Mouse Brain in Stereotaxic Coordinates, Third Edition (Elsevier Academic Press).

Perciavalle V, Apps R, Bracha V, Delgado-García JM, Gibson AR, Leggio M, Carrel AJ, Cerminara N, Coco M, Gruart A, and Sánchez-Campusano R (2013). Consensus paper: current views on the role of cerebellar interpositus nucleus in movement control and emotion. Cerebellum 12, 738–757. [PubMed: 23564049]

Rizzi G, Coban M, and Tan KR (2019). Excitatory rubral cells encode the acquisition of novel complex motor tasks. Nat. Commun 10, 2241. [PubMed: 31113944]

Rossi J, Balthasar N, Olson D, Scott M, Berglund E, Lee CE, Choi MJ, Lauzon D, Lowell BB, and Elmquist JK (2011). Melanocortin-4 receptors expressed by cholinergic neurons regulate energy balance and glucose homeostasis. Cell Metab. 13, 195–204. [PubMed: 21284986]

Roth BL (2016). DREADDs for Neuroscientists. Neuron 89, 683–694. [PubMed: 26889809]

Ruder L, Takeoka A, and Arber S (2016). Long-Distance Descending Spinal Neurons Ensure Quadrupedal Locomotor Stability. Neuron 92, 1063–1078. [PubMed: 27866798]

Ruigrok TJ (2012). Handbook of the Cerebellum and Cerebellar Disorders (Springer).

Saueressig H, Burrill J, and Goulding M (1999). Engrailed-1 and netrin-1 regulate axon pathfinding by association interneurons that project to motor neurons. Development 126, 4201–4212. [PubMed: 10477289]

Schouenborg J, Weng HR, Kalliomäki, J., and Holmberg, H. (1995). A survey of spinal dorsal horn neurones encoding the spatial organization of withdrawal reflexes in the rat. Exp. Brain Res 106, 19–27. [PubMed: 8542974]

Sherrington CS (1911). The integrative action of the nervous system (Yale University Press).

Sherrington CS, and Laslett EE (1903). Observations on some spinal reflexes and the interconnection of spinal segments. J. Physiol 29, 58–96. [PubMed: 16992657]

Shik ML, and Orlovsky GN (1976). Neurophysiology of locomotor automatism. Physiol. Rev 56, 465–501. [PubMed: 778867]

Shik ML, Severin FV, and Orlovskiǐ GN (1966). [Control of walking and running by means of electric stimulation of the midbrain]. Biofizika 11, 659–666. [PubMed: 6000625]

Skinner RD, Coulter JD, Adams RJ, and Remmel RS (1979). Cells of origin of long descending propriospinal fibers connecting the spinal enlargements in cat and monkey determined by horseradish peroxidase and electrophysiological techniques. J. Comp. Neurol 188, 443–454. [PubMed: 114558]

Sperry RW (1950). Neural basis of the spontaneous optokinetic response produced by visual inversion. J. Comp. Physiol. Psychol 43, 482–489. [PubMed: 14794830]

Sprague JM, and Chambers WW (1953). Regulation of posture in intact and decerebrate cat. I. Cerebellum, reticular formation, vestibular nuclei.J. Neurophysiol 16, 451–463. [PubMed: 13097194]

Strick PL, Dum RP, and Fiez JA (2009). Cerebellum and nonmotor function. Annu. Rev. Neurosci 32, 413–434. [PubMed: 19555291]

Sybirska E, and Górska T (1980). Effects of red nucleus lesions on forelimb movements in the cat. Acta Neurobiol. Exp. (Warsz.) 40, 821–841. [PubMed: 7234514]

Tervo DGR, Hwang B-Y, Viswanathan S, Gaj T, Lavzin M, Ritola KD, Lindo S, Michael S, Kuleshova E, Ojala D, et al. (2016). A Designer AAV Variant Permits Efficient Retrograde Access to Projection Neurons. Neuron 92, 372–382. [PubMed: 27720486]

Thach WT, Goodkin HP, and Keating JG (1992). The cerebellum and the adaptive coordination of movement. Annu. Rev. Neurosci 15, 403–442. [PubMed: 1575449]

Thomas DM, Kaufman RP, Sprague JM, and Chambers WW (1956). Experimental studies of the vermal cerebellar projections in the brain stem of the cat (fastigiobulbar tract). J. Anat 90, 371–385. [PubMed: 13345716]

Tolbert DL, Bantli H, Hames EG, Ebner TJ, McMullen TA, and Bloedel JR (1980). A demonstration of the dentato-reticulospinal projection in the cat. Neuroscience 5, 1479–1488. [PubMed: 7402481]

Ueno M, Nakamura Y, Li J, Gu Z, Niehaus J, Maezawa M, Crone SA, Goulding M, Baccei ML, and Yoshida Y (2018). Corticospinal Circuits from the Sensory and Motor Cortices Differentially Regulate Skilled Movements through Distinct Spinal Interneurons. Cell Rep. 23, 1286–1300.e7. [PubMed: 29719245]

Uno M, Kozlovskaya IB, and Brooks VB (1973). Effects of cooling interposed nuclei on tracking-task performance in monkeys. J. Neurophysiol 36, 996–1003. [PubMed: 4202615]

Uusisaari MY, and Knöpfel T (2012). Diversity of neuronal elements and circuitry in the cerebellar nuclei. Cerebellum 11, 420–421. [PubMed: 22278661]

Uusisaari M, Obata K, and Knöpfel T (2007). Morphological and electrophysiological properties of GABAergic and non-GABAergic cells in the deep cerebellar nuclei. J. Neurophysiol 97, 901–911. [PubMed: 17093116]

Vardy E, Robinson JE, Li C, Olsen RHJ, DiBerto JF, Giguere PM, Sassano FM, Huang X-P, Zhu H, Urban DJ, et al. (2015). A New DREADD Facilitates the Multiplexed Chemogenetic Interrogation of Behavior. Neuron 86, 936–946. [PubMed: 25937170]

Voogd J, and Koehler PJ (2018). Historic notes on anatomic, physiologic, and clinical research on the cerebellum. Handb. Clin. Neurol 154, 3–26. [PubMed: 29903448]

Wang X, Liu Y, Li X, Zhang Z, Yang H, Zhang Y, Williams PR, Alwahab NSA, Kapur K, Yu B, et al. (2017). Deconstruction of Corticospinal Circuits for Goal-Directed Motor Skills. Cell 171, 440–455.e14. [PubMed: 28942925]

Wang Z, Maunze B, Wang Y, Tsoulfas P, and Blackmore MG (2018). Global Connectivity and Function of Descending Spinal Input Revealed by 3D Microscopy and Retrograde Transduction. J. Neurosci 38, 10566–0581. [PubMed: 30341180]

Watson C, Paxinos G, and Kayalioglu G (2009). The Spinal Cord (Academic Press).

Wenner P, and O'Donovan MJ (1999). Identification of an interneuronal population that mediates recurrent inhibition of motoneurons in the developing chick spinal cord. J. Neurosci 19, 7557–7567. [PubMed: 10460262]

Whishaw IQ, and Gorny B (1996). Does the red nucleus provide the tonic support against which fractionated movements occur? A study on forepaw movements used in skilled reaching by the rat. Behav. Brain Res 74, 79–90. [PubMed: 8851917]

Whishaw IQ, Whishaw P, and Gorny B (2008). The structure of skilled forelimb reaching in the rat: a movement rating scale. J. Vis. Exp 816, 816.

Wiesendanger M (1969). The pyramidal tract: recent investigations on its morphology and function. Ergeb. Physiol 61, 72–136. [PubMed: 4983201]

Wilson VJ, Uchino Y, Maunz RA, Susswein A, and Fukushima K (1978). Properties and connections of cat fastigiospinal neurons. Exp. Brain Res 32, 1–17. [PubMed: 207546]

Wolpert DM, Miall RC, and Kawato M (1998). Internal models in the cerebellum. Trends Cogn. Sci 2, 338–347. [PubMed: 21227230]

Wu Z, Autry AE, Bergan JF, Watabe-Uchida M, and Dulac CG (2014). Galanin neurons in the medial preoptic area govern parental behaviour. Nature 509, 325–330. [PubMed: 24828191]

Xue M, Atallah BV, and Scanziani M (2014). Equalizing excitation-inhibition ratios across visual cortical neurons. Nature 511, 596–600. [PubMed: 25043046]

Yu J, and Eidelberg E (1981). Effects of vestibulospinal lesions upon locomotor function in cats. Brain Res. 220, 179–183. [PubMed: 6168331]

Yu J, and Eidelberg E (1983). Recovery of locomotor function in cats after localized cerebellar lesions. Brain Res. 273, 121–131. [PubMed: 6616217]

Zackowski KM, Thach WT Jr., and Bastian AJ (2002). Cerebellar subjects show impaired coupling of reach and grasp movements. Exp. Brain Res 146, 511–522. [PubMed: 12355280]

Zhu H, Pleil KE, Urban DJ, Moy SS, Kash TL, and Roth BL (2014). Chemogenetic inactivation of ventral hippocampal glutamatergic neurons disrupts consolidation of contextual fear memory. Neuropsychopharmacology 39, 1880–1892. [PubMed: 24525710]

Highlights

- Cerebellospinal (CeS) neurons constitute approximately 5%–10% of excitatory deep cerebellar neurons

- Ipsilateral CeS neurons to the cervical cord are necessary for skilled forelimb movement

- Contralateral CeS neurons (CeS$^{cer\text{-}contra}$) are necessary for skilled locomotor learning

- CeS$^{cer\text{-}contra}$ neurons target local and long-range neurons in the cervical cord
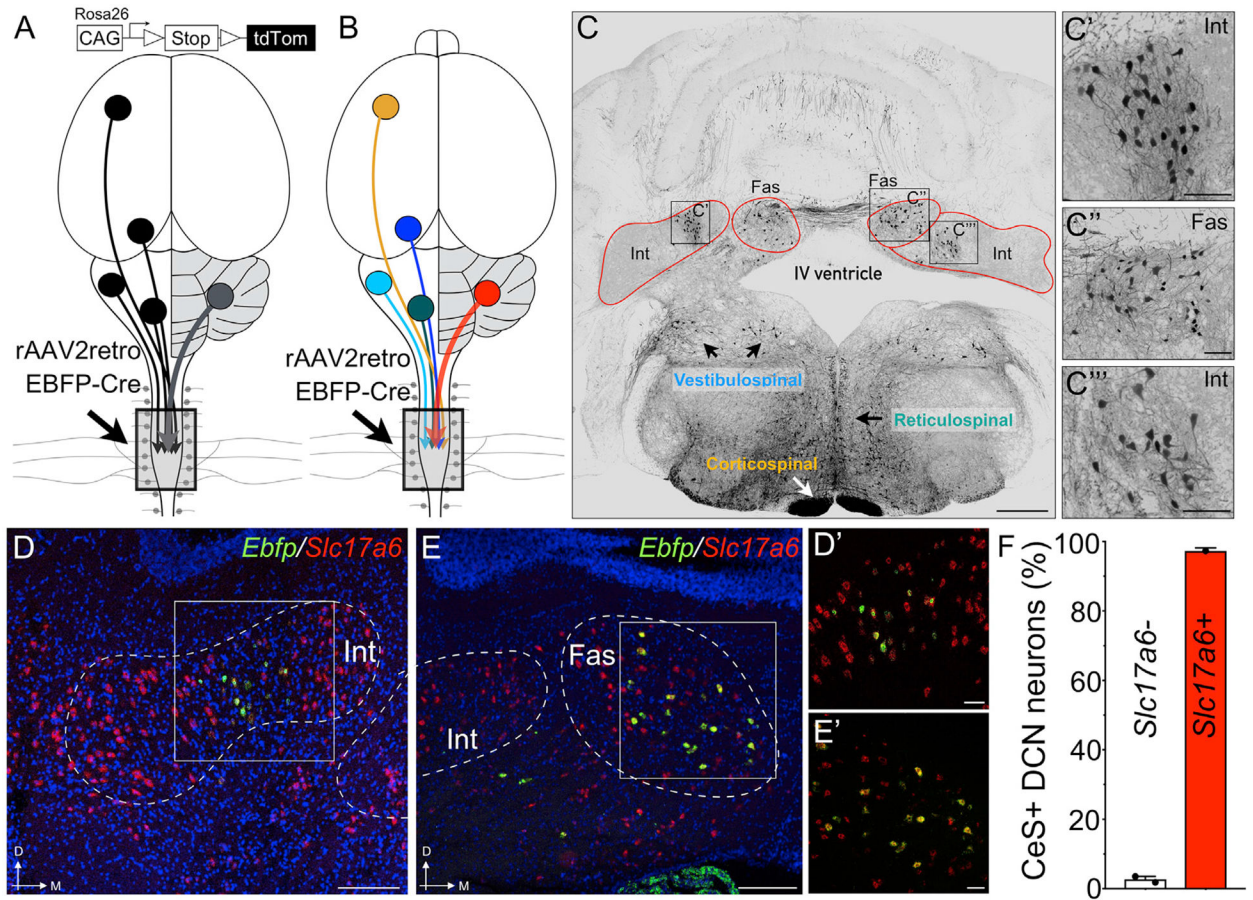
Figure 1. A Direct Excitatory Projection from the DCN to the Spinal Cord

(A and B) Experimental strategy for labeling pre-spinal neurons. Predicted (A) and observed (B) pre-spinal pathways are highlighted.

(C) Coronal section showing pre-spinal neurons in the DCN (fastigial and interpositus) (outlined in red) and the brainstem. Also highlighted (arrows) are descending pathways, including the vestibulospinal, reticulospinal, and corticospinal pathways. C′, C″, and C‴ are higher magnification images of boxed areas.

(D-F) Excitatory nature of cerebellospinal (CeS) neurons. Coronal sections (from mice with intraspinal injections of rAAV2-retro: EBFP-Cre) showing colocalization of *Ebfp* (green) and *Slc17a6*/vGlut2 (red) mRNA in CeS neurons of the interpositus (D) and fastigial (E) nuclei. Quantification of percentage of CeS neurons (*Ebfp⁺*) with *Slc17a6* (red bar) or without *Slc17a6* (white bar) (F). A total of 367 *Ebfp*-expressing neurons from two mice were analyzed. Individual values and mean ± SEM are shown.

Scale bars, 500 μm (C); 100 μm (C′–C‴); 200 μm (D and E); 50 μm (D′ and E′). Stitched, Z-projected images are shown in (C), (D), and (E). Also see Figure S1.
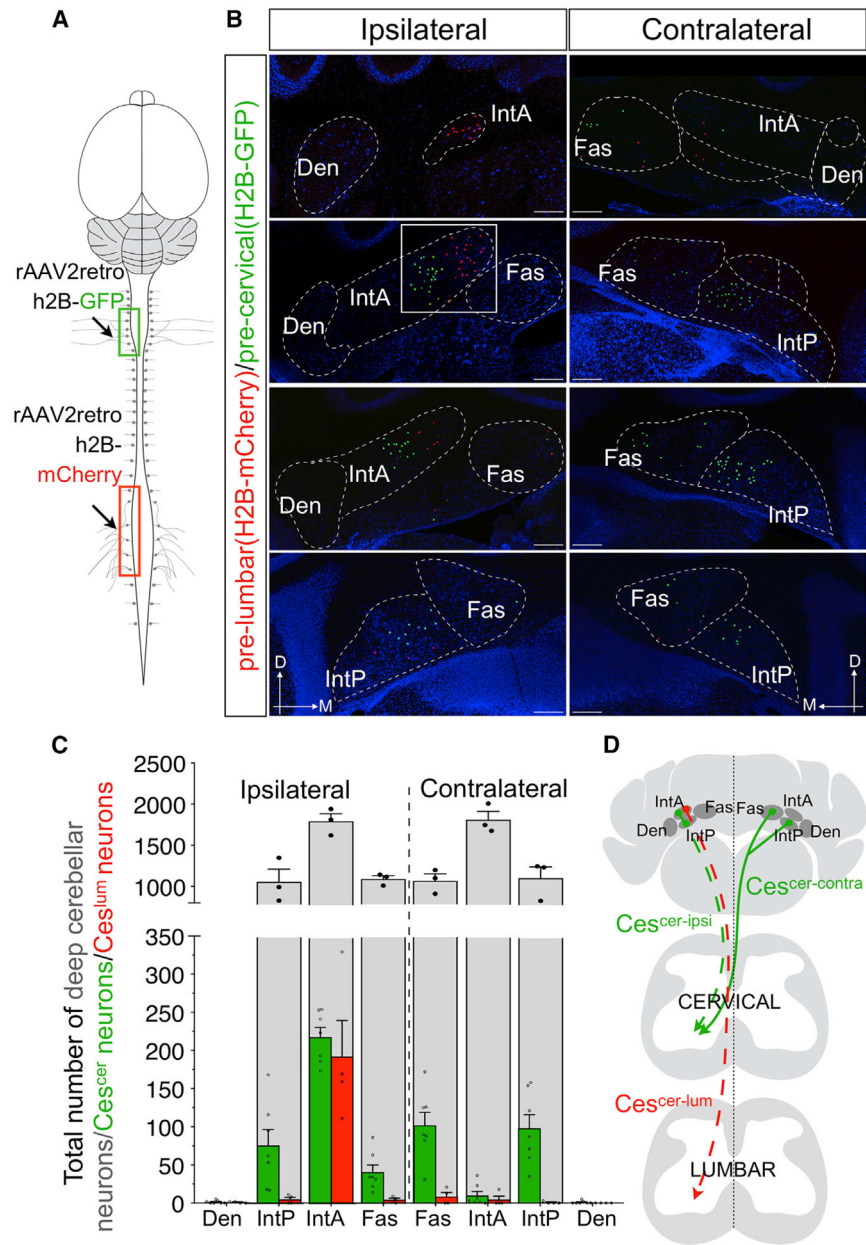
Figure 2. Anatomical Organization of CeS Neurons

(A) Experimental strategy for visualizing pre-cervical (CeS^{cer}) and pre-lumbar (CeS^{lum}) CeS neurons.

(B) Rostro-caudal (top-bottom) coronal sections showing retrolabeled GFP$^+$ CeS^{cer} neurons (green) and mCherry$^+$ CeS^{lum} neurons (red) in the DCN (outlined). Boxed area in row 2 shows anatomical segregation of CeS^{cer} and CeS^{lum} neurons in the IntA. Stitched, Z-projected images are shown.

(C) Quantification of total number of neurons (gray, n = 3 mice, dentate excluded) and the total number of CeS^{cer} (green, n = 7 mice) or CeS^{lum} (red, n = 4 mice) neurons in the respective DCN (~20 sections per mouse). Individual values and mean ± SEM are shown.

(D) Summary schematic depicting the main anatomical subdivisions of CeS neurons.

Scale bar, 200 μm. See also Figures S1 and S2.

Figure 3. CeS^cer-ipsi Neurons Are Required for Skilled Reaching

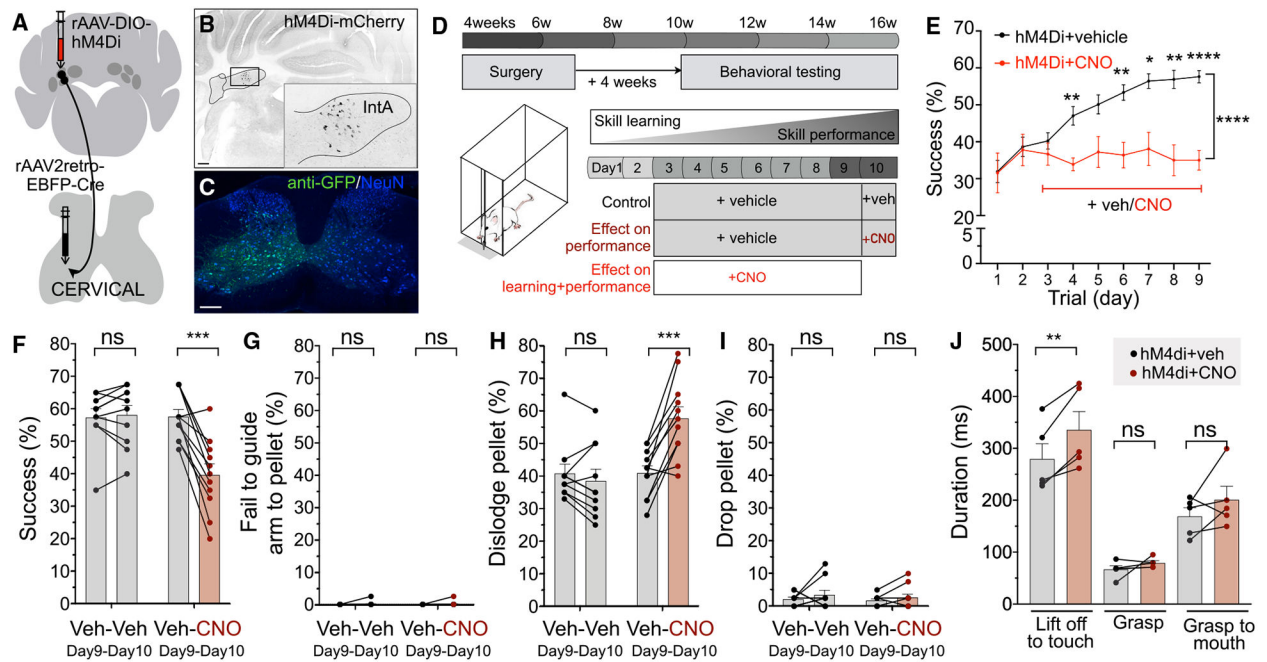(A) Experimental strategy for expressing hM4Di specifically in CeS^cer-ipsi neurons. (B and C) Specificity of viral-labeling strategy. Representative sections showing specific expression of hM4Di-mCherry in the ipsilateral DCN

(B) and unilateral expression of EBFP-Cre (immunostained with anti-GFP antibody) in the cervical spinal cord (C). Stitched, Z-projected images are shown.

(D) Schematic depicting the experimental timeline for behavioral testing and single-pellet retrieval.

(E) Reduced rate of success in animals treated with CNO (red, n = 9 mice) during the learning/execution phase as compared to vehicle-treated controls (black, n = 21 mice) (two-way ANOVA).

(F–I) Control mice (black) in (E) were treated with either vehicle (n = 10 mice) or CNO (n = 11 mice) on day 10 to assess the effect of silencing on performance post-learning. Quantification of the percentage of successful trials (F) and three types of failed trials (G–I) (fail to guide arm to the pellet in G, dislodge pellet in H, drop pellet in I) on day 10 compared to day 9 for each mouse (vehicle treated in black and CNO treated in maroon, paired t test).

(J) Quantification of duration of the three different phases of the trial in (F–I) (n = 5 mice). Phase1: liftoff to establishing contact with the pellet or dislodging the pellet; Phase2: grasping or manipulation of the pellet; Phase 3: lifting pellet to mouth (paired t test).

Scale bar, 200 μm (B and C). Mean ± SEM and/or individual values are shown. *p < 0.05; **p < 0.01; ***p < 0.001; ****p < 0.0001; n.s., not significant. See also Figure S3 and Videos S1, S2, and S3.
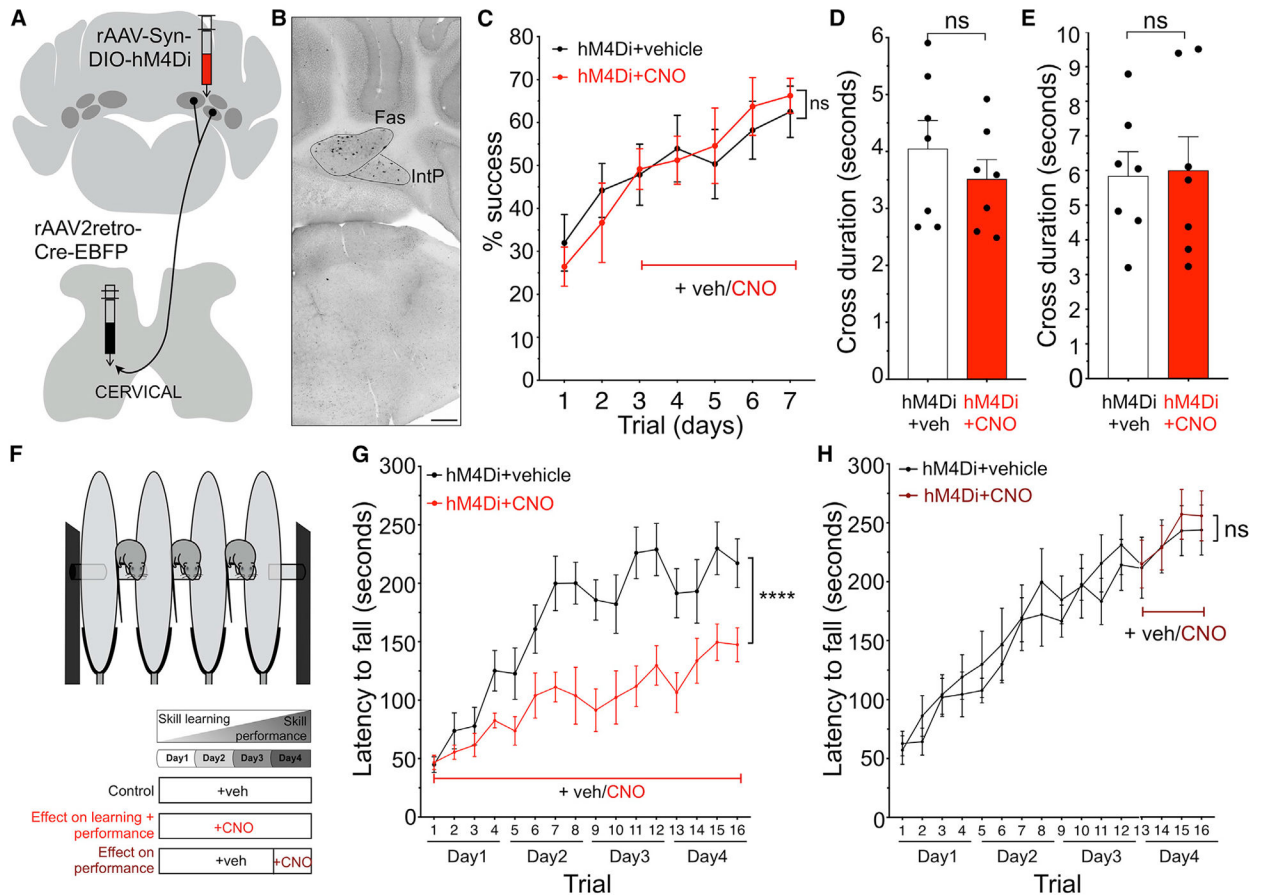
Figure 4. CeS^cer-contra Neurons Are Important for Skilled Locomotor Learning

(A) Experimental strategy for expressing hM4Di specifically in CeS^cer-contra neurons.

(B) Specificity of viral-labeling strategy. Stitched, Z-projected images are shown.

(C) Similar rate of successful pellet retrievals in a single-pellet retrieval task. Vehicle (n = 7 mice) or CNO (n = 6 mice) was delivered throughout the learning/performance phase (days 3–7) of skilled reaching task (two-way ANOVA).

(D and E) Similar performance in beam-walk task. Mice were tested on wide (D) and narrow (E) beams before (white bars) or after (red bars) CNO delivery, and the time taken to cross a 0.7-m section of the beam was measured (n = 7 mice, paired t test).

(F) Schematic depicting rotarod behavioral testing.

(G) Quantification showing reduced rotarod performance (presented as latency to fall) in mice treated with CNO (n = 9 mice) (red) on days 1–4 (learning/performance phase) as compared to vehicle-treated controls (n = 10 mice) (two-way ANOVA).

(H) Similar rotarod performance upon CNO-delivery post-learning. Quantification of latency to fall in animals treated with vehicle during days 1–3 of rotarod testing, followed by either vehicle (n = 7) or CNO (maroon, n = 8) on day 4, revealed no significant differences between both groups (two-way ANOVA).

Scale bar, 200 μm (B). *p < 0.05; **p < 0.01; ***p < 0.001; ****p < 0.0001; n.s., not significant. Mean ± SEM and/or individual values are shown. See also Figure S4.
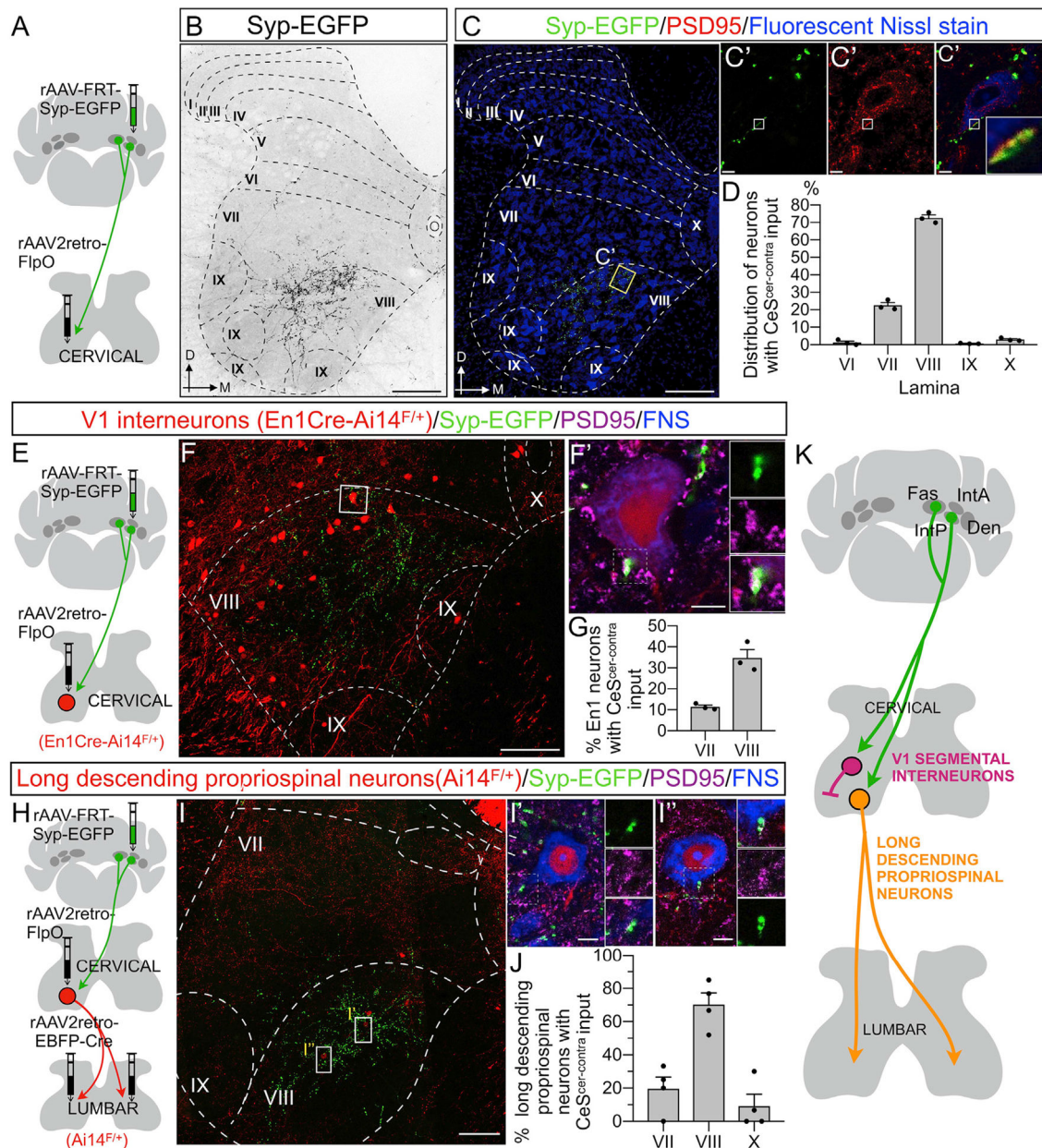
Figure 5. CeS^cer-contra Neurons Target Specific Neuronal Populations in Laminae VII and VIII in the Ventral Horn of the Cervical Spinal Cord

(A) Experimental strategy for visualizing synaptic terminals of CeS^cer-contra neurons.

(B and C) Transverse section through the cervical spinal cord showing the distribution of synaptic terminals in laminae VII and VIII of the spinal cord (rendered in black in B and green in C). Higher-magnification image (C′–C‴) (single optical slice, ~1 μm thick) of a boxed neuron (C) shows close apposition of synaptic terminals of CeS^cer-contra neurons (green) and post-synaptic density (PSD95, red) of a spinal neuron.

(D) Quantification of the relative distribution of spinal neurons that receive synaptic input from CeS^cer-contra neurons in laminae VI–X (4–7 sections per mouse were analyzed, n = 3

mice). (E) Experimental strategy for visualizing CeS$^{cer-contra}$ synaptic contacts onto En1-lineage neurons (in En1-Cre; Ai14$^{F/+}$ mice).

(F) Transverse section through the cervical spinal cord showing CeS$^{cer-contra}$ synaptic terminals (green) onto En1-lineage neurons (red). Higher-magnification image (F′) (single optical section) of a boxed neuron.

(G) Quantification of the percentage of En1-lineage neurons in laminae VII and VIII that receive synaptic input from CeS$^{cer-contra}$ neurons (4–7 sections per mouse were analyzed, n = 3 mice).

(H) Experimental strategy for visualizing CeS$^{cer-contra}$ synaptic contacts onto long descending propriospinal (LDP) neurons (in Ai14$^{F/+}$ mice).

(I) Transverse section through the cervical spinal cord showing CeS$^{cer-contra}$ synaptic terminals (green) onto LDP neurons (red). Higher magnification images (I′ and I″) (single optical section) of two individual boxed neurons.

(J) Quantification of the percentage of LDP neurons in laminae VII, VIII, and X that receive synaptic input from CeS$^{cer-contra}$ neurons (6–9 sections per mouse were analyzed, n = 4 mice).

(K) Schematic depicting CeS$^{cer-contra}$ inputs onto segmental V1-lineage neurons and intersegmental LDP neurons.

Mean ± SEM and individual values are shown. Rexed laminae are indicated. Stitched, Z-projected images are shown in (B), (C), (F), and (I). Scale bars, 200 μm (B and C); 5 μm (C′); 100 μm (F); 5 μm (F′); 100 μm (I); 10 μm (I′ and I″). See also Figure S5.
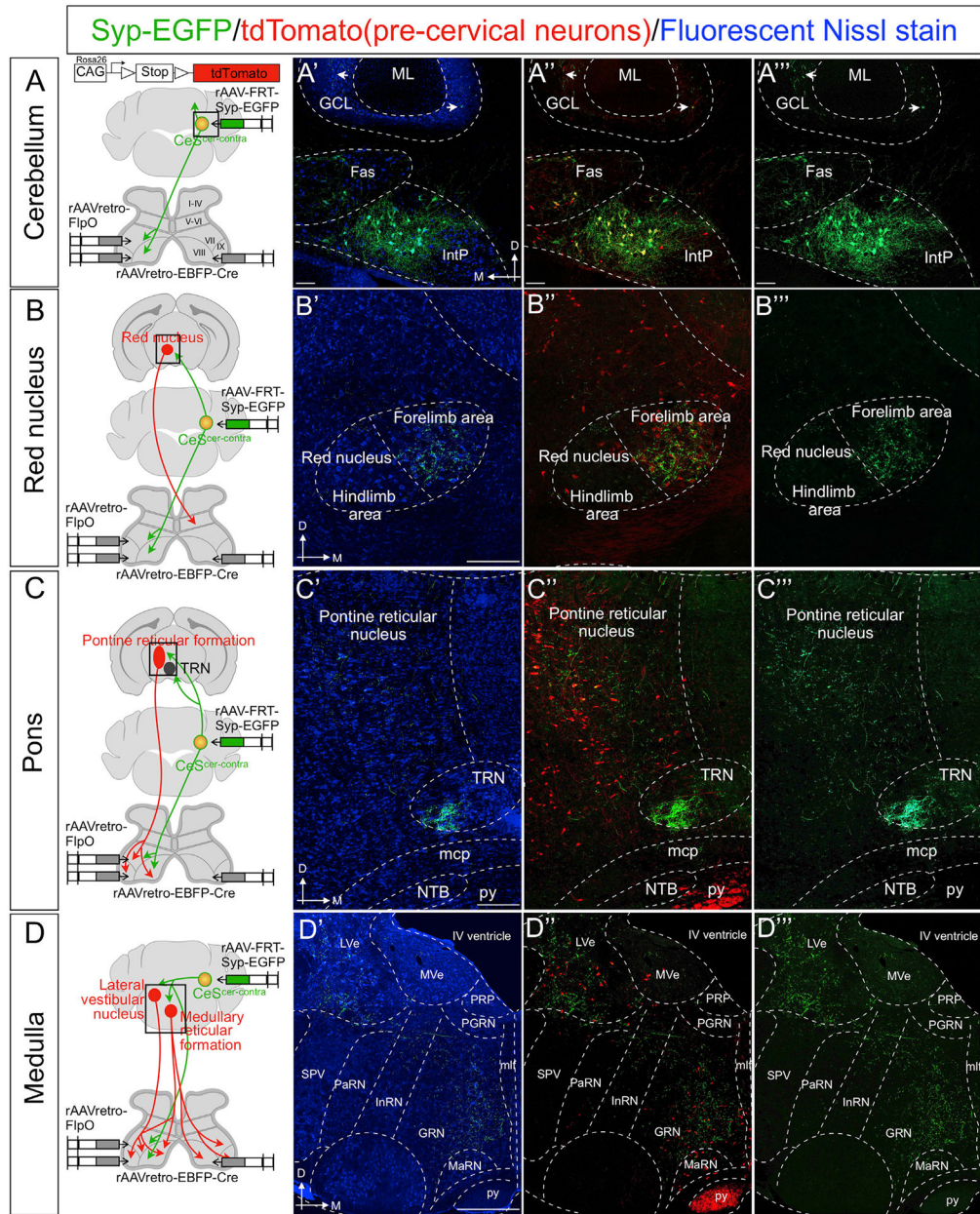
Figure 6. CeS^{cer-contra} Neurons Target Sources of Major Descending Pathways

Experimental strategy for visualizing CeS$^{cer-contra}$ synaptic terminals (green) against a background of labeled pre-cervical neurons (red). Coronal sections showing soma of CeS$^{cer-contra}$ neurons (red and green) in the IntP and fastigial nuclei and synaptic terminals of CeS$^{cer-contra}$ neurons (green) in the cerebellar cortex (arrows) (A–A′). Coronal sections showing CeS$^{cer-contra}$ terminals in the region occupied by pre-cervical rubrospinal neurons in the red nucleus (B); reticulospinal neurons and pontine reticulotegmental nucleus (TRN) in the pontine reticular formation (C); and reticulospinal neurons in the gigantocellular nucleus and vestibulospinal neurons in the LVe (D).

Fluorescent Nissl stain (blue) was used to delineate the various nuclei. Images are representative of results from four mice. InRN, intermediate reticular nucleus; LVe, lateral

vestibular nucleus; MaRN, magnocellular reticular nucleus; mcp, middle cerebellar peduncle; MVe, medial vestibular nucleus; NTB, nucleus of the trapezoid body; PGRN, paragigantocellular nucleus; PRP, nucleus prepositus; py, pyramids; SPV, spinal nucleus of the trigeminal. Scale bars, 100 μm (A); 200 μm (B and C); 500 μm (D). Stitched, Z-projected images are shown. See also Figure S6.

KEY RESOURCES TABLE

REAGENT or RESOURCE	SOURCE	IDENTIFIER
Antibodies		
NeuN	Millipore Sigma	ABN90; RRID:AB_2298772
ChAT	Millipore Sigma	AB144P
PSD95	ThermoFisher	51–6900; RRID:AB_2533914
EBFP/GFP	Rockland	600–101–215; RRID:AB_218182
Chx10	Abeam	Ab16141; RRID:AB_302278
NeuroTrace™ 640/660 Deep-Red Fluorescent Nissl stain	Thermofisher Scientific	N21483; RRID:AB_2572212
NeuroTrace™ 435/455 Blue Fluorescent Nissl Stain	Thermofisher Scientific	N21479, RRID:AB_2572212
Bacterial and Virus Strains		
AAV2retro-hSyn-h2B-mCherry	This paper	N/A
AAV2retro-hSyn-h2B-EGFP	This paper	N/A
AAV2retro-pmSyn1-EBFP-Cre	(Madisen et al., 2015)	RRID: Addgene_51507
AAV-hSyn-DIO-HM4Di-mCherry	(Krashes et al., 2011)	RRID: Addgene_44362
AAV-hSyn-dF-HA-KORD-IRES-mCitrine	(Vardy et al., 2015)	RRID: Addgene_65417
AAV1-hSyn-mCherry-DIO-DTA	UNC Viral Vector Core	AV6239B
AAV-hSyn-DIO-mCherry	This paper	N/A
AAV-hSyn-mCherry	This paper	N/A
AAV-hSyn-FLPo	Xue et al., 2014	RRID: Addgene_60663
AAV-hSyn-FSF-Syp-EGFP	This paper	N/A
Critical Commercial Assays		
RNAscope Fluorescent Multiplex Reagent Kit	ACD	320850
Experimental Models: Organisms/Strains		
Mouse: Ai14 B6.Cg-GT(ROSA) 26Sor$^{tm14(CAG-tdTomato)HZe}$/J	Jackson Laboratory	Jax007914
Mouse: En1:Cre En1$^{tm2(cre)/Wrst}$/J	Jackson Laboratory	Jax 007916
Mouse: ChatCre Chat$^{tm2(cre)Lowl}$/J	Jackson Laboratory	Jax 006410